AD_____

Award Number: **W81XWH-11-1-0609**

TITLE: **Identification of miRNA Signatures Associated with Epithelial Ovarian Cancer Chemoresistance with Further Biological and Functional Validation of Identified Key miRNAs**

PRINCIPAL INVESTIGATOR: **Analisa DiFeo**

CONTRACTING ORGANIZATION: Mount Sinai School of Medicine, New York
New York, New York 10029-6574

REPORT DATE: August **2012**

TYPE OF REPORT: **Annual Report**

PREPARED FOR: U.S. Army Medical Research and Materiel Command
Fort Detrick, Maryland 21702-5012

REPORT DOCUMENTATION PAGE

Form Approved
OMB No. 0704-0188

1. REPORT DATE *(DD-MM-YYYY)*	2. REPORT TYPE	3. DATES COVERED *(From - To)*
August 2012	Annual	15 July 2011-14 July 2012

4. TITLE AND SUBTITLE

Identification of miRNA Signatures Associated with Epithelial Ovarian Cancer Chemoresistance with Further Biological and Functional Validation of Identified Key miRNAs

5a. CONTRACT NUMBER

5b. GRANT NUMBER
W81XWH-11-1-0609

5c. PROGRAM ELEMENT NUMBER

6. AUTHOR(S)

Analisa DiFeo, Christine Lee

5d. PROJECT NUMBER

5e. TASK NUMBER

5f. WORK UNIT NUMBER

8. PERFORMING ORGANIZATION REPORT NUMBER

7. PERFORMING ORGANIZATION NAME(S) AND ADDRESS(ES)

Mount Sinai School of Medicine, New York
New York, New York 10029-6574

9. SPONSORING / MONITORING AGENCY NAME(S) AND ADDRESS(ES)

U.S. Army Medical Research and Materiel Command
Fort Detrick, Maryland 21702-5012

10. SPONSOR/MONITOR'S ACRONYM(S)

11. SPONSOR/MONITOR'S REPORT NUMBER(S)

12. DISTRIBUTION / AVAILABILITY STATEMENT

Approved for public release; distribution unlimited

13. SUPPLEMENTARY NOTES

14. ABSTRACT

Epithelial ovarian cancer (EOC) is the most lethal gynecologic malignancy in the United States. One major obstacle in the clinical management of the disease is the high incidence of recurrence after cytotoxic chemotherapy and the development of platinum resistance. Given the crucial importance to overcome chemotherapy resistance to platinum therapy, we hypothesize that miRNA profiling in EOC cell lines and surgical specimens with varying chemosensitivities will uncover a potential predictive "fingerprint" for individualized therapy, while further biological validation of these miRNAs signatures will allow for the development of novel therapeutic strategies to enhance chemosensitivity. Through mircoarray analysis of miRNAs differentially expressed in an *in vitro* model of acquired carboplatin resistance consisting of EOC cell lines sensitive to carboplatin, A2780, and its resistant variants, CP20 (moderately resistant) and CP70 (resistant), we identified a panel of miRNAs that correlate with carboplatin response. We uncovered four miRNAs (miR-23b, miR-132, miR-183 and miR-203) that are significantly upregulated in both platinum-resistant cell lines. Additionally, we have also correlated their expression with several clinical parameters in a cohort of ovarian tumor specimens from women diagnosed with stage III, grade 3, papillary serous adenocarcinoma all treated with platinum-based chemotherapy. Through this analysis we found that miR-183 correlated with patient survival. The median survival for patients with high expression of miR-183 was 27.2 months versus 53.8 months for those who have low miR-183 expression. In summary, in the 5 months period which we had this grant we were able to validate the dysregulation of several miRNAs in platinum resistant cell lines as well as uncover a novel miRNA that correlates with ovarian cancer patient survival.

15. SUBJECT TERMS
microRNA, ovarian cancer, platinum resistance

16. SECURITY CLASSIFICATION OF:			17. LIMITATION OF ABSTRACT	18. NUMBER OF PAGES	19a. NAME OF RESPONSIBLE PERSON
					USAMRMC
a. REPORT U	b. ABSTRACT U	c. THIS PAGE U	UU	82	19b. TELEPHONE NUMBER *(include area code)*

Standard Form 298 (Rev. 8-98)
Prescribed by ANSI Std. Z39.18

Table of Contents

Page

Introduction……..…..**4**

BODY……..5

Key Research Accomplishments…….…….. **8**

Reportable Outcomes…… **9**

Conclusion…… **10**

References……**11**

Appendices……**11**

Introduction

Epithelial ovarian cancer (EOC) is the most lethal gynecologic malignancy. Platinum and taxane-based drugs are used in combination as first-line chemotherapeutics for women newly diagnosed with EOC, unfortunately approximately 20% do not respond to this treatment and have very poor outcomes due to chemoresistance, making advanced ovarian cancer particularly difficult to eradicate. Given the crucial importance to overcome chemotherapy resistance to platinum therapy, we hypothesize that miRNA profiling in EOC cell lines and surgical specimens with varying chemosensitivities will uncover a potential predictive "fingerprint" for individualized therapy, while further biological validation of these miRNAs signatures will allow for the development of novel therapeutic strategies to enhance chemosensitivity. The overarching goal of this project is to identify miRNAs involved in the development of ovarian cancer chemoresistance and ascertain their biological relevance using both *in vitro* and *in vivo* models of ovarian adenocarcinoma. To test our hypothesis, we propose to: 1) Validate the clinical relevance of the miRNA signature we identified in our *in vitro* model of chemosensitivity using a well-defined clinical cohort of ovarian cancer specimens; 2) determine the biological and functional relevance of the miRNAs that correlate with chemotherapeutic response**;** 3) explore whether *in vivo* targeting of miRNAs that are overexpressed in chemoresistant cancer cells can sensitize chemoresistant ovarian tumors to platinum treatment and inhibit ovarian cancer dissemination in a pre-clinical ovarian cancer mouse model. Our study, if successful, will identify key miRNAs involved in the regulation of chemoresistance in EOC and significantly contribute to the understanding of their biology and function *in vitro* and *in vivo*. Those miRNAs may also serve as predictive markers for tailored therapy. Furthermore, targeting these miRNAs using *in vivo* will provide a new paradigm for overcoming chemotherapy resistance clinically and thus improve survival in late stage disease.

BODY

*This report includes the data obtained in only **5 months** because I transferred to another institution shortly after this award was issued. We are currently in the process of getting the remaining funding transferred to my current institution were I will continue the studies.*

Through miRNA array analysis of an *in vitro* model of acquired platinum resistance consisting of an OvCa cell line sensitive to carboplatin, A2780, and its resistant variants, CP20 (moderately resistant) and CP70 (resistant) which, we have identified a panel of miRNAs that are correlated with carboplatin response (Tables 1&2)(abstract presented at SGO 2011 attached). Interestingly, the majority of miRNAs were upregulated in the platinum resistant variants compared to the parental sensitive cell line. Well-known miRNA clusters such as the miR-17-92 and the let7 family were some the most significantly altered miRNAs. Additionally, we both the moderately resistant and resistant cell lines had many of the same dysregulated miRNAs with only a few miRNA that were exclusively changed in each cell line alone (Figure 1).

Table 1: miRNAs downregulated in platinum resistant ovarian cancer cells

Mature ID	FC (CP20/ A2780)	p-value	FC (CP70/A2780)	p-value
miR-92a	0.44	0.008	0.23	0.0005
miR-18a	0.79	0.04	0.19	0.00009
miR-210	0.25	0.004	0.41	0.01
miR-124	0.3	0.008	0.2	0.004
miR-125b	0.45	0.01	0.14	0.003
miR-363	0.11	0.02	0.13	0.03
miR-130a	0.4	0.002	0.73	0.08
miR-193a-5p	0.5	0.08	0.8	0.36
miR-20a	0.56	0.06	0.15	0.005
miR-19a	0.57	0.07	0.15	0.008
miR-17	0.61	0.11	0.16	0.01

Figure 1

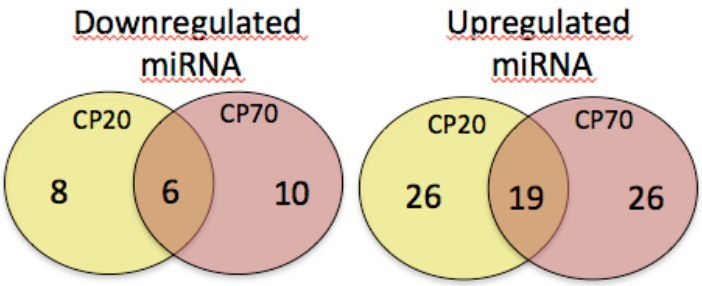

Table 2: miRNAs upregulated in platinum resistant ovarian cancer cells

Mature ID	FC (CP20/ A2780)	p-value	FC (CP70/ A2780)	p-value
let-7g	26.32	0.000026	50.97	0.000021
let-7b	6.11	0.000046	23.4	0.000568
let-7i	2.9	0.000078	7.74	0.000072
let-7e	8.18	0.001984	15.91	0.000152
let-7a	6.42	0.003078	13.72	0.002556
miR-132	**15.73**	**0.000028**	**9.33**	**0.000391**
miR-23b	**15.94**	**0.000037**	**10.69**	**0.000328**
miR-9	**36.04**	**0.00003**	**38.54**	**0.000007**
miR-148a	8.64	0.000251	7.97	0.000083
miR-7	9.57	0.000011	3.18	0.003136
miR-27b	8.03	0.001567	3.92	0.001501
miR-148b	3.19	0.001814	3.69	0.005809
miR-30c	3.23	0.001991	2.21	0.010526
miR-200c	7.79	0.002082	5.74	0.002728
miR-183	**6.64**	**0.003117**	**9.07**	**0.000999**
miR-146b-5p	9.44	0.004059	4.52	0.020673
miR-196a	3.87	0.007077	3.45	0.005725
miR-193b	4.81	0.010541	4.93	0.010036
miR-128	3.86	0.016774	4.56	0.01578
miR-181c	2.81	0.006823	2	0.111084
miR-214	**3.81**	**0.025935**	**2.18**	**0.361897**
miR-181a	**1.97**	**0.048522**	**1.54**	**0.127733**
miR-181d	**2.03**	**0.048564**	**1.08**	**0.953417**
miR-181b	**1.59**	**0.053891**	**1**	**0.89711**
miR-199a-3p	2.2	0.000754	1.01	0.973468
miR-21	2.51	0.002247	1.2	0.15501
miR-126	1.65	0.053338	3.32	0.000606
miR-125a-5p	1.84	0.077812	2.05	0.041421
miR-100	3.03	0.08162	4.13	0.013408
miR-191	1.46	0.210084	1.83	0.034618
miR-29a	0.87	0.519884	1.86	0.032717
miR-15b	1.64	0.000377	2.79	0.000285
let-7d	2.21	0.477048	6.13	0.008461

In task 1 (months 1-3), we sought to confirm our array findings and validate the clinical relevance of the panel of miRNA's identified using a well-defined clinical cohort of ovarian cancer specimens. Firstly, in order to confirm the miRNA array results several of the significantly upregulated miRNAs which have not been previously associated with chemotherapy response were analyzed in the panel of platinum-resistant ovarian cancer cell lines. Taqman PCR analysis confirmed that 4 (miR-203, -183, -23b and -132) of the 5 (miR-203, -183, -23b, -132 and -7) miRNAs analyzed were significantly upregulated in the platinum-resistant cells (Figure 2). In addition, rather then comparing two distinct groups (i.e., sensitive vs. resistant), we directly correlated the level of each miRNA expression with the IC50 of each cell lines which is a measure of the effectiveness of platinum in inducing apoptosis. As shown in Figure 3, the expression of miR-203, -183, -23b and -132 reveal a positive linear correlation with cell resistance. Strikingly, miR-132 expression displays an almost perfect correlation with cell resistance ($R^2 > 0.98$).

Figure 2

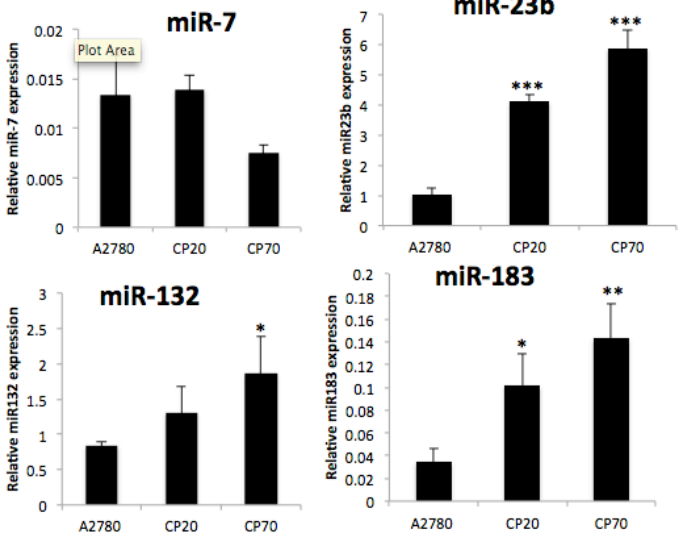

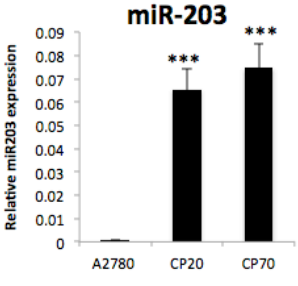

Figure 3

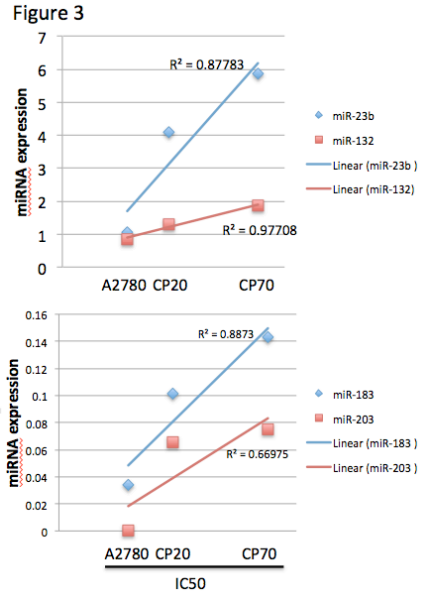

Next, in order to assess the clinical relevance of these miRNA we ascertained whether there was a correlation between miRNA expression and several clinical parameters including progression-free survival and overall survival. Total RNA was extracted using RecoverAll Total Nucleic Acid isolation kit (Ambion) from a well annotated clinical cohort of 53 stage III serous adenocarcinoma patient samples all treated with platinum therapy. Using the median expression value for each miRNA as a cut-point, the cohort was dichotomized into miRNA-high or miRNA-low expressing tumors. Interestingly, only miR-183 showed a trend towards significance with survival, high expression of miR-183 correlated with poor overall survival (Figure 4). Specifically, tumors with high expression of miR-183 had a median survival of 27.2 months whereas those patients who has low expression the median survival was 53.8 months (p=0.056, 95% CI 1.4-2.6).

Figure 4

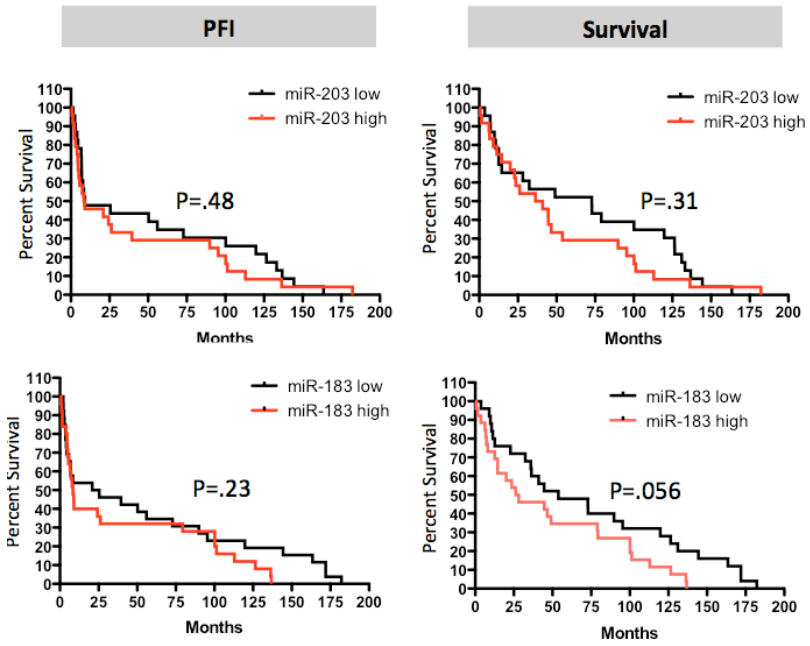

We are currently looking to expand these studies and have obtained a second clinical cohort from Dr. Stefanie Avril at the Technical University Munich in order to increase the power of the study by including more patient samples. To date we have completed Task 1 but will continue to evaluate the expression of other miRNAs that were found to be differentially expressed in platinum resistant cell lines as well as determine whether there is a miRNA signature that correlates with patient outcome rather then individual miRNAs. In task 2, we are going to determine the functional relevance of these miRNAs that correlate with platinum resistance and patient outcome. Unfortunately, as we were preparing to characterize ovarian cancer cells that exogenously express miR-183 my laboratory transferred institutions and we were unable to complete the rest of the studies. We are currently in the process of transferring this grant to my new institution and we plan on continuing to complete tasks 2 and 3.

Key Research Accomplishments:

- Uncovered a miRNA signature that correlates with platinum resistance
- Majority of aberrant miRNAs are common among the moderately and completely resistant ovarian cancer cell lines
- miR-203, -183, -23b and -132 directly correlate with platinum sensitivity in ovarian cancer cell lines
- miR-183 is potentially novel prognostic biomarker for advanced-stage ovarian cancer

Reportable outcomes:

Abstracts:

1) Fishman D, Wang F, DiFeo A and Narla G Quantitative PCR array identification of microRNA clusters associated with epithelial ovarian cancer chemoresistance. Gynecologic Oncology 120 (2011) S2–S133

Manuscripts:

1) Parikh A, Lee C, Joseph P, Marchini S, Baccarini A, Kolev V, Fruscio R, Shah H, Mullokandov, Fishman D, Romualdi C, D'Incalci M, Rahaman J, Kalir T, Redline RW, Brown BD, Narla G, and DiFeo A miR-181a induces TGF-β-mediated epithelial-to-mesenchymal transition and promotes epithelial ovarian cancer progression. Cell Reports, *In revision*

2) Purnell R, Lee C, Down JD, Menon N and DiFeo A. A Reflectance Based Method for Label Free Detection of Low Abundance MicroRNA Biomarkers. Nano Letters, *In review*

Employment:

1) Promoted to a tenure-tracked Assistant Professor at the Case Comprehensive Cancer Center, Case Western Reserve University, Cleveland, OH

Conclusion

Epithelial ovarian cancer (EOC) is the most lethal gynecologic malignancy. Platinum and taxane-based drugs are used in combination as first-line chemotherapeutics for women newly diagnosed with EOC, unfortunately approximately 20% do not respond to this treatment and have very poor outcomes due to chemoresistance, making advanced ovarian cancer particularly difficult to eradicate. The overarching goal of this project is to identify miRNAs involved in the development of ovarian cancer chemoresistance and ascertain their biological relevance using both *in vitro* and *in vivo* models of ovarian adenocarcinoma. In the 5 months that we had this grant, prior to transferring to another institution we were able to complete Specific Aim 1 and uncover novel miRNAs involved in ovarian cancer chemotherapy resistance. Specifically, we found that both the moderately resistant and resistant ovarian cancer cells have similar miRNA profiles. Additionally, we validated several of the dysregulated miRNAs found through the microarray platform and confirmed that the expression of miR-203, -183, -23b and -132 directly correlate with platinum sensitivity. Lastly, through the analysis of a well-annotated clinical cohort of advanced-stage ovarian cancer, we found that high expression of miR-183 correlates with decreased patient survival, suggesting that it may be a potential prognostic biomarker for advanced stage ovarian cancer.

Although numerous miRNA profiling studies including our own have uncovered miRNAs that correlate with ovarian cancer patient outcome[1-5] or platinum resistance[6-8] and suggest a link between miRNA signature and chemoresistance, the discrepancy between reported resistance-associated miRNA signatures, the lack of biological validation and functional targets represents major hurdles in understanding miRNAs role in modulating ovarian cancer chemotherapy response. Therefore, in Specific Aims 2 we will functionally validate all miRNAs that show a correlation with patient outcome using both gain- and loss-of-function experiments in a panel of ovarian cancer cell lines with varying sensitivity to platinum therapy. Lastly, in Specific Aim #3 we will access whether the miRNAs that have a biological effect on ovarian cancer cells can be used as a therapeutic target using either miRNA mimic or antigomers. Ultimately, upon receipt of this grant to my current institution we will (1) continue to expand our miRNA signature with ultimate goal of uncovering a potential predictive “fingerprint” for individualized therapy based on miRNA expression, (2) functionally validate the miRNAs that are clinically relevant, and (3) therapeutically target miR-183 and other miRNAs that correlate with patient outcomes.

Our study, if successful, will identify key miRNAs involved in the regulation of chemoresistance in EOC and systemically validate their biology and function in relevant cell culture and in vivo models of the disease. Targeting these miRNAs using lentiviral based sponge vectors may provide a new paradigm for overcoming chemotherapy resistance clinically and thus improve survival in late stage disease.

References

1. Croce CM, *Cancer Res September 15, 2007 67; 8699*

2. Yang N, et al. MicroRNA microarray identifies Let-7i as a novel biomarker and therapeutic target in human epithelial ovarian cancer. Cancer Res. 2008;68(24):10307-10314.

3. Dahiya N, et al. MicroRNA expression and identification of putative miRNA targets in ovarian cancer. PLoS One. 2008;3(6):e2436.

4. Delfino KR and Rodriguez-Zas SL. Transcription factor-miRNA-Target Gene Networks Associted with Ovarian Cancer Survival and Recurrence. PLOS One 2013;8(3):e58608.

5. Lee H, Park CS, Deftereos G, Morihara J, Stern JE, Hawes SE, Swisher E, Kiviat NB, Feng Q. MicroRNA Expression in Ovarian Carcinoma and Its Correlation with Clinicopathological Features. World J Surg Oncol 2012 Aug 27;10:174.

6. Sorrentino A, et al. Role of microRNAs in drug resistant ovarian cancer cells. Gynecol Oncol. 2008;111(3):478-486.

7. Kumar S, Kumar A, Shah PP, Rai SN, Panguluri SK, Kakar SS. MicroRNA Signature of Cisplatin Resistant vs. Cis-Platin Sensitive Ovarian Cancer Cell Lines. J Ovarian Res. 2011 Sep 22;4(1):17.

8. Yang L, Li N, Wang H, Jia X, Wang X, Luo J. Altered microRNA expression in cisplatin-resistant ovarian cancer cells and upregulation of miR-130a associated with MDR1/P-glycoprotein-mediated drug resistance. Oncol Rep. 2012;28(2):592-600.

untreated cells from each using high-resolution mass spectrometry. Raw mass spectrometric data were processed and analyzed for variations in the spectral counts of peptides between sample sets and bioinformatics was accomplished using Ingenuity Pathways Analysis (IPA).

Results: The total numbers of proteins and peptides identified are listed in the table. Cisplatin-treated UWB1.289 cells had 458 upregulated and 748 downregulated proteins compared with untreated cells, with a spectral count difference ≥2. A group of molecules associated with an oxidative stress response pathway were noted to be significantly upgraded compared with the untreated line. This pathway includes nine molecules involved in cellular defense responses to oxidative stress, and two molecules in this pathway are inhibited by cisplatin. It is not significantly upregulated within the BRCA1-restored cell line after treatment. Following cisplatin treatment of the UWB1.289 + BRCA cell line, there was a significant upregulation of caspase signaling factors, which are involved in apoptosis and cleavage of DNA damage sensors. This pathway is downregulated in UWB1.289-treated cells.

Conclusions: BRCA1 dysfunction is an important factor in the response to treatment with platinum for patients with EOC. Our results indicate that a number of auxiliary protein signaling pathways are activated in BRCA1-deficient EOC cell lines in response to cisplatin exposure. Specifically, upregulation of oxidative stress pathway molecules and inhibition of caspase-induced cleavage of DNA damage sensors within the BRCA1-deficient cell line may represent mechanisms of compensation for inadequate DNA repair.

	UWB1.289 No treatment	UWB1.289 Cisplatin	UWB1.289 + BRCA1 No treatment	UWB1.289 + BRCA1 Cisplatin
Proteins	2,482	2,221	2,438	2,160
Peptides	23,964	21,980	22,395	21,199

doi:10.1016/j.ygyno.2010.12.130

124

Quantitative PCR array identification of microRNA clusters associated with epithelial ovarian cancer chemoresistance

D. Fishman, F. Wang, A. DiFeo, G. Narla
Mt. Sinai School of Medicine, New York, NY

Objective: Despite improved chemotherapy regimens, chemoresistance remains a challenge for the treatment of epithelial ovarian cancer (EOC). Meanwhile, effective biomarkers to predict an individual's response to a distinct therapy are lacking. In the present study, we aimed to identify chemoresistant EOC-associated microRNA (miRNA) signature and explore the possibility of developing a miRNA-based novel therapeutic strategy to overcome chemoresistance.

The expression profile of 88 cancer-related miRNAs was determined using a 96-well plate cancer RT2 miRNA PCR array from SA Biosciences in an in vitro cell culture model composed of ovarian cancer cell line A2780 (sensitive) and its cisplatin-resistant variants CP20 (moderately resistant) and CP70 (resistant) (Fig. A). Total RNA was extracted using the TRIzol reagent (Invitrogen) and reverse transcribed using the RT2 miRNA First Strand Kit from SA Biosciences.The resulting cDNA was then diluted, mixed with 2× RT2 SYBR Green PCR Master Mix (SA Biosciences), and loaded into the wells of a PCR array plate to allow real-time PCR amplification and detection. Data analysis was performed with the Web-based software package for the miRNA PCR array system. Cells undergoing apoptosis were measured by FACS on cisplatin treatment to determine the apoptotic index.

Results: Among the 88 miRNAs profiled, 15 were significantly overexpressed in CP70 cells and 7 were significantly downregulated in CP70 cells as compared with A2780 (absolute fold change >5, $P<0.05$). Hierarchical clustergram analysis was performed to show the cluster of those miRNAs (Fig. B). Correlation analysis of the expression of those miRNAs with the apoptotic index of A2780, and its resistant variants, CP20 and CP70, revealed a panel of miRNAs associated with cisplatin response. Of those miRNAs that are overexpressed in cisplatin-resistant cell lines (CP20 and CP70) as compared with A2780, 7 showed a positive linear correlation with cell resistance (Fig. C) ($R^2>0.9$). Of the 7 miRNAs that were significantly downregulated in CP70 cells, 5 (miR-17, -18a, -19a, -20a, and -125b) showed a negative linear correlation with chemoresistance (Fig. D) ($R^2>0.9$), among which miR-17 displayed a perfect correlation ($R^2=0.9999$).

Conclusions: Our results suggest the complexity of miRNA regulation in chemoresistance, and the miRNA panels identified in our preliminary study open a new avenue for the study of miRNA biology and function evaluation in chemoresistance.

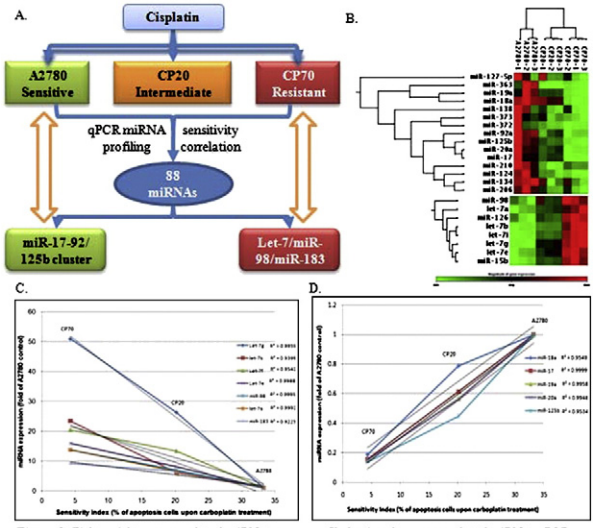

Figure 1. Eighty-eight cancer-related miRNAs were profiled using the cancer-related miRNA qPCR array from SA bioscience. **A.** Schematic view of our *in vitro* model for miRNA profiling in OvCa cell lines of varied response to cisplatin. **B.** Clustergram view of representative miRNAs identified to be differentially expressed in sensitive OvCa cells and its resistant variants. Note, miR-17-92 cluster miR-125b and let-7/miR-98 are shown clustered together. **C.** miRNAs that are positively correlated with EOC resistant phenotype to cisplatin. **D.** miRNAs that are negatively correlated with EOC resistant phenotype to cisplatin. The miRNA expression in **C. and D.** was presented as fold of that in A2780 (y-axis) against the sensitivity of each cell line (x-axis).

doi:10.1016/j.ygyno.2010.12.131

125

Stop and smell the volatile organic compounds: A novel breath-based bioassay for detection of ovarian cancer

A. Nick, R. Stone, J. Bottsford-Miller, P. Ramirez, C. Tung, G. Armaiz-Pena, E. Felix, A. Sood
University of Texas M.D. Anderson Cancer Center, Houston, TX

Objective: The high mortality rate of ovarian carcinoma is attributed in part to the lack of an adequately sensitive screening modality. Breath analysis offers a painless, noninvasive technique of separating and identifying volatile hydrocarbons using gas chromatography/

microRNA-181a regulates epithelial-mesenchymal transition and promotes ovarian cancer dissemination

Aditya Parikh[1,11], Christine Lee[1,10,11], Peronne Joseph[10], Sergio Marchini[5], Alessia Baccarini[1], Valentin Kolev[3], Chiara Romualdi[8], Robert Fruscio[6,7], Hardik Shah[1], Feng Wang[3], Gavriel Mullokandov[1], David Fishman[3], Maurizio D'Incalci[5,7], Jamal Rahaman[3], Tamara Kalir[4], Raymond W. Redline[9], Brian D. Brown[1], Goutham Narla[1,2,10], and Analisa DiFeo[1,10*]

[1]The Department of Genetics and Genomic Sciences, [2]Department of Medicine, [3]Department of Obstetrics and Gynecology, and [4]Department of Pathology, The Mount Sinai School of Medicine, New York, N.Y. 10029. [5]Department of Oncology, Mario Negri Institute for Pharmacological Research, Milano, Italy. [6]Clinic of Obstetrics and Gynecology, University of Milano-Bicocca, San Gerardo Hospital, Monza, Italy. [7]MaNGO Group, Milano, Italy. [8]The Department of Biology, Universtià degli studi di Padova. [9]The Department of Pathology, University Hospitals Case Medical Center, and [10]Case Comprehensive Cancer Center, Case Western Reserve University, Cleveland, OH 44106.

[11] These authors contributed equally to this manuscript.

*Address for correspondence:

Analisa DiFeo, Ph.D.

Case Comprehensive Cancer Center

Case Western Reserve University

2103 Cornell Road

Cleveland, OH 44106

Email: analisa.difeo@case.edu

***No conflicts of interest to disclose**

ABSTRACT

Ovarian cancer is the most lethal gynecological cancer primarily due to advanced stage of disease at diagnosis. Effective therapeutic targets and prognostic biomarkers are still lacking due to insufficient knowledge of the pathways that regulate ovarian cancer progression. Here, we identify miR-181a as a mediator of disease dissemination through the induction of EMT and direct activation of the TGF-β signaling pathway via repression of its functional target Smad7. High expression of miR-181a and phospho-Smad2 were associated with poor patient outcome and were enriched in recurrent compared to matched-primary tumors. Ectopic expression of miR-181a resulted in increased cellular survival, migration, drug resistance, and *in vivo* tumor burden and dissemination. Conversely, targeting this miRNA using a decoy vector resulted in significant decreases in cell survival, migration, invasion, and MET in ovarian cancer cell lines. Combined, our findings provide new insights into the molecular functions of miR-181a and reveal its critical role in ovarian cancer pathogenesis.

Significance: Understanding the mechanisms that regulate EOC dissemination is crucial in order to improve patient survival. Our data identifies miR-181a as a modulator of ovarian cancer dissemination through the induction of EMT and highlights its role as a potential biomarker and therapeutic target for aggressive late-stage ovarian cancer.

INTRODUCTION

In the United States, approximately 22,300 women are diagnosed with ovarian cancer and approximately 15,500 die from the disease every year (1). Epithelial ovarian cancer (EOC), which accounts for ~90% of all ovarian cancers, has the highest mortality rate among all gynecological malignancies. This is primarily due to advanced stage at diagnosis and the recurrence of chemotherapy resistant tumors, resulting in poor overall survival in the majority of patients (1,2). An incomplete understanding of the molecular pathways that regulate disease development poses one of the greatest challenges to improving clinical outcome. Hence, elucidating functionally relevant molecular drivers of ovarian cancer progression is crucial for the development of targeted therapy that can help improve survival outcomes in affected patients.

Epithelial-to-mesenchymal transition (EMT) plays a critical role in metastasis and is associated with chemotherapy resistance. EMT is characterized by loss of epithelial morphology and reorganization of cytoskeleton rendering epithelial cells more motile and invasive through up- and down-regulation of several molecules including tight, adherent junction proteins and mesenchymal markers. Interestingly, several studies have indicated TGF-β to function either as a tumor suppressor or as a promoter inducing EMT, cell motility and invasion depending on cellular context. Understanding the mechanisms of how TGF-β signaling is modulated could identify key molecular drivers of dissemination and provide potential molecular targets for drug development.

microRNAs (miRNA) are small noncoding RNA molecules that negatively regulate gene expression at the post-transcriptional level in a sequence-specific manner,

primarily via base pairing to the 3' untranslated region (3'UTR) of the target mRNA transcripts. Mounting evidence implicates miRNAs as regulators of the tumor phenotype through their ability to modulate the expression of critical genes and signaling networks involved in tumorigenesis and the downstream malignant processes (3,4). Numerous miRNA profiling studies in EOC have identified miRNAs associated with chemotherapy resistance and disease progression (5-10). In a study analyzing 443 advanced epithelial ovarian cancer specimens from The Cancer Genome Atlas it was found that high expression of miR-181a was associated with shorter recurrence time (23 months vs. 59 months, P=0.013), possibly implicating a significant role for this miRNA in ovarian cancer pathogenesis (11). In addition, miR-181a expression has been shown to be regulated by numerous signaling networks including TGF-β, MYC, estrogen, STAT3 and Wnt/β-catenin, indicating a potential role in regulating cancer relevant signaling pathways (12-15). Lastly, miR-181a-1 resides in the 1q "hot spot" region of gain (1q31.3-1q32.1) (16), which is overexpressed in ovarian carcinomas compared to normal tubal epithelium and ovarian surface epithelium (17).

In this study, we identify miR-181a as an inducer of TGF-β-mediated EMT via suppression of Smad7 in ovarian cancer and define a unique mechanism by which the TGF-β signaling pathway is activated in EOC tumors. Our data highlights a novel functional role of miR-181a in ovarian cancer biology and uncovers a potential prognostic biomarker and molecular target for the treatment of EOC.

Results

Elevated expression of miR-181a in advanced stage EOC

In order to assess the clinical relevance of miR-181a in EOC, we analyzed its expression in a clinically annotated patient cohort of high-grade stage III primary papillary serous ovarian cancer by Taqman-based quantitative real time PCR (qRT-PCR). Using the median expression value of miR-181a as a cut-point, the cohort was dichotomized into miR-181a-high or miR-181a-low expressing tumors. The median progression-free survival (PFS) was 59.9 months for patients with low miR-181a expression, whereas in patients with high levels of miR-181a the median PFS was 7.1 months (Fig. 1A). Furthermore, patients with low miR-181a levels exhibited a median overall survival (OS) of 66.6 months in contrast to a median OS of 24.9 months in patients with high expression levels of miR-181a (Fig. 1A). Given the association of miR-181a and clinical outcome, we next sought to determine if other miRNAs that have been previously reported to be overexpressed in EOC, specifically miR-183 and miR-203, had similar correlations with outcome in our clinical cohort (18). Kaplan-Meier analysis revealed that neither miRNA correlated with disease progression (Fig. S1). In addition, tumors of patients with PFS<6 months (clinically described as platinum resistant) had higher expression of miR-181a (*P*=0.01) when compared to patients with PFS>6 months (platinum sensitive) (Fig. 1B). Taken together, these data support the association between high miR-181a expression and poor patient outcome.

miR-181a promotes epithelial-to-mesenchymal transition (EMT)

Given the clinical evidence of its association with both poor progression-free and overall survival, we assessed the functional role of miR-181a in ovarian cancer biology. We stably expressed miR-181a (p181a), an empty vector (pBABE), and a vector expressing a mutant form of miR-181a (p181a mut) in the A2780 cell line (derived from

chemotherapy naïve primary epithelial ovarian tumor), which expresses the lowest relative levels of miR-181a in a panel of ovarian cancer cell lines (Fig. 1C). The miR-181a expression in the two independently derived polyclonal pools of miR-181a-transduced cells (p181a#1 and p181a#2) was comparable to its basal expression in the other ovarian cancer cell lines as well as patient samples (Fig. 1C). Functional assessment of the exogenous miR-181a was achieved using a lentiviral-based miRNA sensor vectors carrying the mCherry reporter gene with either four miR-181a binding sites in the 3'UTR or no binding site, serving as a transduction control (Fig. S2). Only p181a#1 and p181a#2 cells exhibited strong down-regulation of reporter expression when infected with the mCherry-based miR-181a sensor, confirming enhanced expression of functionally active miR-181a (Fig. S2). Ectopic expression of miR-181a resulted in a fibroblast-like mesenchymal appearance of cells with loss of epithelial features consistent with EMT (Fig. 1D). These morphological features were consistent with defined molecular alterations that occur during the induction of EMT as demonstrated by decreased expression of epithelial markers, E-cadherin and Keratin 8, and a concomitant increase in the expression of mesenchymal markers, N-cadherin, fibronectin, and Col3A1 (Fig. 1E). The miR-181a-induced EMT-like features were also observed in an additional ovarian serous adenocarcinoma cell line, HEY (Fig. S3). EMT plays an important role in cell motility, cellular survival, drug response, and tumor dissemination *in vivo*; therefore, we next assessed whether miR-181a-induced EMT affected these biological processes. Colony formation assay revealed that enhanced miR-181a expression increased cellular survival and conferred platinum resistance without affecting cell proliferation (Figs. 1F, 1G, and Fig. S4). Additionally, both trans-well migration and wound healing assays showed that miR-181a overexpression significantly increased cellular motility (Figs. 1H and 1I). Lastly, we examined the effects of miR-181a on ovarian cancer dissemination in a pre-clinical intraperitoneal mouse

model of late stage disease. Three weeks after intraperitoneal injection of miR-181a-overexpressing or pBABE cells, miR-181a-overexpressing cells formed a greater number of disseminated nodules within the peritoneal cavity (Fisher's Exact test, *P*=0.01; OR: 47.67; 95% CI: 1.6-1424) which correlated to increased overall tumor burden (*P*=0.03) (Fig. 1J), indicating that tumor cells with elevated levels miR-181a had acquired a propensity to disseminate and survive *in vivo*. qRT-PCR confirmed overexpression of miR-181a and transcriptional changes in EMT markers in these tumors (Figs. 1K and 1L).

Inhibition of miR-181a suppresses migration and cellular survival

A tough decoy (TuD) vector specific to miR-181a was utilized to determine the impact of miR-181a inhibition on EMT-driven phenotypes (19,20). The SKOV3 ovarian cancer line, which has relatively high expression levels of miR-181a, was stably transduced with either the TuD-miR-181a (miR-181a Decoy) or TuD-miR-331.3p (control decoy) vector. Cells transduced with TuD-miR-181a exhibited decreased expression levels of miR-181a when compared to cells transduced with TuD-miR-331.3p (Fig. 2A). In addition, the mCherry miR-181a sensor reporter vector confirmed a more than 80% inhibition of miR-181a function (Fig. 2B).

Stable inhibition of miR-181a led to differences in morphology and marker gene expression consistent with MET (mesenchymal-epithelial transition), wherein the cells reverted from a more spindle-like morphology to an epithelial-like phenotype (Fig. 2C). Western blot analysis confirmed a significant increase in the epithelial marker (E-cadherin) and a decrease in mesenchymal markers (N-cadherin and Col3A1) (Fig. 2C).

Furthermore, miR-181a inhibition led to a decrease in cellular survival (Fig. 2D) and rendered the cells less migratory (Fig. 2E).

miR-181a is a novel modulator of the TGF-β signaling pathway

To identify the cellular pathways modulated by miR-181a and define specific targets driving the observed EMT phenotype, we performed high-throughput RNA sequencing (Illumina) on A2780 pBABE and p181a cell lines with a combination of computational target prediction, global transcriptome- and pathway-based analysis. Using a threshold of a minimum fold change ≥ 5 or fold change ≤ 5 (with $P \leq 0.05$), we identified a total of 739 differentially expressed genes: 705 downregulated and 34 upregulated (Table S1-2). The high-throughput mRNA sequencing data revealed alterations in the epithelial and mesenchymal markers consistent with global activation of an EMT-like genetic program (Table 1). Interestingly, nearly 7% of significantly downregulated genes had a putative miR-181a binding site(s) as predicted by TargetScan (Table S1). We next utilized the Ingenuity Pathway Analysis (IPA) software (Ingenuity, Inc.) to further define potential targets and the major pathways/networks driving the miR-181a-mediated EMT phenotypes. The transforming growth factor-β signaling pathway was the most significantly dysregulated pathway, among those with significant number of genes altered by greater than 5-fold (P=1.1x10^{-4}) (Fig. 3A).

TGF-β is among several growth factors that can act as inducers of EMT and has been found to play an important role in cancer invasion and metastasis (21-23). Thus, we sought to explore the role of miR-181a in the regulation of TGF-β signaling in ovarian cancer. Given that the R-Smads, Smad2 and Smad3, are key intracellular mediators of

cellular responses to TGF-β signaling, we assessed the effects of miR-181a expression on the phosphorylation of Smad2 (P-Smad2) and Smad3 (P-Smad3). In both stable cell lines expressing miR-181a, P-Smad2 and P-Smad3 expressions were increased with a concomitant decrease in the inhibitory Smad, Smad7 (Fig. 3B). Consistent with the activation of the TGF-β signaling pathway, the activin receptor (ACVR2A) and the type I TGFβ receptor (TGFβ-RI), which are also putative targets of miR-181a, were also increased in miR-181a expressing cells (Fig. 3B). Next, we utilized both a TGF-β /activin-responsive p3TP reporter and the artificial SBE4-luc reporter in order to assess TGF-β transcriptional response (24). We found that miR-181a overexpression induced both p3TP and SBE4 reporter activities and conversely, stable inhibition of miR-181a led to a decrease in SBE4 reporter expression by >20% (Figs. 3C and 3D). Furthermore, the addition of a TGF-β RI kinase inhibitor, SB431542, blocked miR-181a-induced phosphorylation of Smad2 (Fig. 3E).

Activation of the TGF-β signaling pathway correlates with poor patient outcome

Given that our data supports a role for miR-181a in regulating TGF-β signaling in ovarian cancer, we next sought to assess whether TGF-β activation and miR-181a expression correlates with EOC disease progression and recurrence in patient samples. The distribution of P-Smad2 positive cells, as well as the intensity of staining, varied depending on PFI and were mainly localized to the nuclei of cancer cells (a marker of activated TGF-β signaling) (Fig. 3F). Overall immune scores in our patient cohort, which were calculated using the Allred scoring system (25), ranged from 0-7 with an overall median score of 2. There was a significant enrichment of P-Smad2 in tumors with shorter time to recurrence (PFI<6 months) (Fisher Exact test; *P=0.016, Table 2).

Furthermore, higher levels of P-Smad2 significantly correlated with shorter median PFI and survival (Fig. 3G) (PFI: P-Smad2 low vs. P-Smad2 high, 55.9 vs. 6.3 **P*=0.01, OR 8.9; 95% CI: 8.3 to 9.4 and survival: P-Smad2 low vs. P-Smad2 high, 79.0 vs. 12.6 ***P*=0.007, OR 6.3; 95% CI: 5.7 to 6.8) (Fig. 3G).

Additionally, Kaplan-Meier analysis revealed that a concomitant decrease in miR-181a and P-Smad2 expression resulted in a significantly prolonged progression-free interval (*P*=0.0007) and overall survival (*P*=0.0006) compared to each biomarker alone (Fig. 3H). Specifically, patient tumors that either had low miR-181a or low P-Smad2 expression had median PFI's of 56 and 53 months, respectively, while in patient tumors with both low miR-181a and P-Smad2 expressions the median PFI doubled to 123 months (****P*=0.0007, OR 18.7; 95% CI: 9.2 to 37.8) (Fig. 3H); differences for OS were similar. Patient tumors expressing either low miR-181a or low P-Smad2 had median survival of 66.6 and 72.8 months, respectively, compared to patient tumors that had both low miR-181a and P-Smad2 expressions in which the median survival doubled to 132.2 months (****P*=0.0006, OR 5.8; 95% CI: 2.6 to 12.8) (Fig. 3H).

In order to further validate the observations that increased miR-181a expression and TGF-β pathway activation correlate with disease progression and recurrence in EOC, we utilized a second clinical cohort of high-grade serous ovarian cancer patients. The expression of miR-181a was assessed in patient- matched tumor biopsies that were taken at primary surgery (PS-O: chemotherapy naïve ovarian tumor) and at secondary surgery (SCR: after tumor has recurred and after at least two lines of chemotherapy). In the SCR tumors, miR-181a expression was upregulated 2.51 fold compared to PS-O (*P*=0.0006) (Figs. 4A and 4B). Additionally, hierarchical bootstrap clustering on the differentially expressed genes (DEG) and analysis of altered biological networks in this

cohort revealed that a subset of SCR tumors (Group A) had a molecular signature indicative of an EMT phenotype driven by TGF-β pathway activation (26), thus making this an ideal cohort to assess whether miR-181a expression was enriched in recurrent tumors specifically with a TGF-β-induced EMT signature. In accordance with all previous data, we observed that the SCR tumors with distinct molecular features of TGF-β-activated EMT (Group A) had elevated miR-181a expression (P=0.0006, Figs. 4A and 4B). Interestingly, in recurrent tumors lacking a distinct EMT signature (Group B), miR-181a was not significantly upregulated (Figs. 4A and 4B). Additionally, in these same tumors there was a significant correlation between the expressions of miR-181a and several EMT markers. Notably, the mesenchymal markers Col5A1 and Col3A1 drew a positive correlation (Col5A1; R=042, p<0.047 and Col3A1; R=0.45, P<0.033) and the epithelial marker, E-cadherin, had a significant inverse correlation with miR-181a expression (E-cadherin; R=-0.44, P<0.03) (Fig. S5).

Smad7 is a direct target of miR-181a and its re-expression can rescue the miR-181a driven phenotypes

We next sought to identify the functional target(s) driving miR-181a-mediated TGF-β pathway activation. The expression of Smad7, a key negative regulator of TGF-β signaling, was decreased ~30-fold in miR-181a-expressing cells (Fig. 5A). Additionally, correlation analysis using miRConnect revealed that Smad7 expression was significantly negatively correlated with miR-181a levels (sPCC = -6.2, Fig. 5A).

To verify that Smad7 is a direct target of miR-181a, a luciferase-based reporter assay using the Smad7 3'UTR was performed (Fig. 5B). Enhanced expression of miR-181a significantly decreased luciferase reporter activity while no change in luciferase

expression was evident in the p181a mut cells as compared to the pBABE control cells (Fig. 5C). Consistent with these results, endogenous levels of Smad7 were also significantly downregulated at both the RNA and protein levels in cells stably expressing miR-181a compared to pBABE or p181a mut cells (Figs. 5D and 3B); this downregulation was also observed in our *in vivo* intraperitoneal tumor tissue (Fig. 5E). Consistent with the notion that miR-181a regulates Smad7 expression, analysis of the matched primary and recurrent ovarian tumors revealed a significant negative correlation (Fig. 5F) ($r = -0.96$, $P<0.0001$) between miR-181a and Smad7 expression, which could reflect our finding that both parameters correlate with tumor recurrence. Conversely, sequestration of miR-181a by the aforementioned decoy vectors abrogated the inhibitory effect of the miRNA on the Smad7 3'UTR reporter constructs and led to an increase in both Smad7 mRNA and protein expression (Figs. 5G and 5H).

Next, we assessed whether Smad7 was the miR-181a target gene that mediated the EMT phenotypes observed. Stable re-expression of Smad7 lacking the 3'UTR was able to attenuate miR-181a-induced EMT as demonstrated by morphological changes, and the relative expression of epithelial and mesenchymal cellular markers E-cadherin, Keratin 8, N-cadherin, and Col3A1 on both the mRNA and protein levels (Figs. 6A, 6B, and 6C). The ability of miR-181a to increase cellular survival and to activate TGF-β signaling was also abrogated (Figs. 6D and 6E).

DISCUSSION

The issues of tumor recurrence, drug resistance, enhanced invasion and metastasis remain a challenge in the treatment and the clinical management of EOC.

Despite a better understanding of EOC genetic alterations in the recent years, our ability to translate these findings into more effective treatments have been limited by the difficulty in identifying functionally relevant drivers of the disease. Because of the inherent heterogeneity and complex nature of EOC (27), known common and highly mutated genes, such as in *TP53* or *BRCA1/2,* have not been successfully exploited in the clinical setting. Hence, identifying molecular drivers of EOC will be crucial to a better understanding of its biology and ultimately for a therapeutic target in advanced stage disease.

Herein, we have identified a single miRNA, miR-181a, that can modulate TGF-β signaling to induce and maintain EMT, and effect further downstream events of tumor cell survival, altered response to chemotherapy, migration, and dissemination *in vivo*. Several studies have demonstrated that TGF-β signaling contributes to ovarian cancer cell plasticity through the regulation of cellular adhesion to the extracellular matrix, thereby increasing cell motility and invasion (28-30). Additionally, ovarian tumors and paired ascites fluid secrete significant amounts of TGF-β (31,32), thus making it imperative to understand the effects of TGF-β on the ovarian tumor biology and the factors that regulate this signaling pathway. In addition, the importance of further understanding the molecular underpinnings involved in TGF-β-induced EMT in EOC was recently highlighted in a comprehensive analysis, which demonstrates that tumors which display a TGF-β-induced mesenchymal signature correlate with poor overall survival (4). Additionally, they uncovered that a miRNA regulatory network, which consisted of a set of 19 miRNA's that were downregulated and inhibited EMT, governed the ovarian cancer mesenchymal phenotype. However, this study does not explore miRNA's that are upregulated in the more aggressive mesenchymal subtype. Our present study provides an understanding of how enhanced expression of miR-181a can confer malignant and

invasive traits through the modulation of a canonical signaling pathway and a consequent maintenance of a mesenchymal state. Furthermore, inhibition of miR-181a led to a reversion of EMT and subsequent events through decreased TGF-β signaling. Our data confirmed Smad7 as a functional target through which TGF-β-mediated EMT occurs; re-expression of Smad7 lacking its 3'UTR was able to rescue miR-181a-mediated phenotypes, deeming Smad7 as a critical mediator of miR-181a-induced EMT. Other recent studies support the crucial role(s) that miRNAs play in mediating EMT and consequent aggressive disease traits. For example, the miR-106b-25 cluster has also been shown to target Smad7 and mediate TGF-β-induced EMT downstream to Six1 in breast cancer (33). MiR-9 directly targets E-cadherin and inhibition of miR-9 had led to an inhibition of metastasis (34). Conversely, the miR-200 and -205 family was shown to target transcriptional repressors of E-cadherin, ZEB1 and SIP1, and re-expression of these miRNAs led to a mesenchymal-to-epithelial transition and prevented TGF-β -induced EMT (35).

The clinical relevance of EMT in ovarian cancer development and progression is not fully understood in part due to conflicting results with EMT marker gene expression patterns and clinical outcomes. For examples, the loss of E-cadherin may correlate with poor survival (36,37) but in an additional large-scale study, the opposite correlation in high grade EOC was observed (38). Our study suggests that the use of biomarkers that regulate EMT, such as miR-181a or P-Smad2, may provide a more functionally relevant prognostic marker. In fact, miRNA expression may be a more accurate classifer of tumor origin and stage than mRNA profiling and standard histological procedures (39). Consequently, we show that the expressions of miR-181a and activated TGF-β signaling, as measured by P-Smad2 expression, significantly correlate with progression-free and overall survivals in a well-annotated advanced stage EOC patient cohort.

Stratifying patients by miR-181a and/or pSmad2 expression in their primary tumor prior to chemotherapy treatment predicted clinical response and survival. Our intraperitoneal in vivo model of late stage EOC also supports that miR-181a increases overall tumor burden with a significantly higher incidence of metastatic nodules in the peritoneum. Importantly, mRNA analyses showed the maintenance of EMT *in vivo* as well as decreased levels of Smad7. The analysis of a second clinical cohort of patient-matched primary and recurrent EOC tumors revealed a significant enrichment of miR-181a expression in recurrent tumors compared to primary chemotherapy naïve tumors. This cohort also confirmed the significant association between miR-181a, Smad7**,** and TGF-β-induced EMT in recurrent tumors (25) with a striking inverse correlation between miR-181a and Smad7 expression. These observations strongly suggest that the pathways that activate miR-181a and in turn leading to Smad7 inhibition are involved in disease progression. Given that enhanced miR-181a expression resulted in activation of other Smad-dependent protein such as TGF-β R1 and potentially non-canonical TGF-β-related pathways, further studies are warranted to explore the functional and clinical relevance of other miR-181a regulated pathways in EOC.

Furthermore, we were able to therapeutically target miR-181a using a decoy vector system and this resulted in significant decreases in cell survival, migration, invasion, and MET in ovarian cancer cell lines highlighting the therapeutic potential of miR-181a silencing in EOC. Additionally, the mechanistic and clinically relevant link between aberrant TGF- β signaling and the SMAD7-miR181 interaction allows for an additional level of targeting with the use of mRNA target protect molecules which block miR-181a binding to the SMAD7 3'utr directly. Ultimately, the development of therapeutics in the context of the miR-181a-TGF-β-Smad7 axis may serve as an efficacious treatment of late stage EOC.

Methods

Analysis of primary human ovarian cancer samples

A de-identified and blinded cohort of 53 primary stage III papillary serous ovarian cancers with long term clinical follow-up was provided by Dr. Jamal Rahaman (Mount Sinai School of Medicine) from an Ovarian Cancer database established with an Institutional human ethics review board approval (IRB # 02-0783, IRB# 02-0668). Total RNA was isolated from duplicate unstained paraffin-embedded sections, which were provided by Dr. Tamara Kalir (Mount Sinai School of Medicine) using the RecoverAll™ Total Nucleic Acid Isolation Kit for FFPE (Life Technologies). Real-time PCR analyses for mRNA and microRNA were performed as described in the RNA extraction and real-time PCR section below. The second patient cohort of EOC was selected from a tumor tissue collection of snap-frozen biopsies recruited at the San Gerardo Hospital in Monza (Italy) and routinely stored at -80°C at the Mario Negri Institute in Milan, (Italy). The cohort comprises 23 stage III-IV patients from whom tumor biopsies were taken at ovary at primary surgery (PS-O), and thus naïve to chemotherapy, and at second surgery for relapse after several lines of chemotherapy (SCR). All clinical and pathological features were recently published (Marchini et al., 2012).

Cell Culture.

We obtained A2780 cells from Dr. Paul Modrich (Duke University), the HEY cells from Gloria S. Huang (Albert Einstein College of Medicine), and SKOV3 cell lines from the American Type Culture Collection and cultivated them in DMEM supplemented with 10% FBS and 1% Penicillin-Streptomycin (recommended media). Cells were cultured in a

humidified atmosphere with 5% CO_2 at 37°C. Trypsin (0.25%)/EDTA solution was used to detach the cells from the culture flask for passaging.

RNA extraction and real-time PCR.

Total RNA was extracted using the miRNeasy kit (Qiagen) according to manufacturer's instructions. For mRNA analysis, complementary cDNA was randomly primed from 1 μg of total RNA using the Fermentas cDNA Synthesis kit. Real-time PCR was subsequently performed in triplicate with 1:15 dilution of cDNA using SYBR green PCR system on the 7900HT Fast real-time PCR machine (Applied Biosciences). Data were collected and analyzed using SDS 2.3 software accompanying the PCR machine. Relative expression levels were determined using the comparative quantification feature of the SDS 2.3 software. All mRNA quantification data were normalized to Actin and 18S. For miRNA analysis, real-time PCR was performed as above using TaqMan microRNA Assay (Applied Biosystems) according to the manufacturer's instructions. TaqMan probes for hsa-miR-181a, miR-16, and RNU6B were purchased from Applied Biosystems. All miRNA data are expressed relative to a RNU6B and/or miR-16, which displayed had stable expression profile throughout all experiments and patient samples.

Generation of A2780 stable cell lines.

MDH1-miR-181a-1-PGK-GFP, a retroviral construct utilized to generate miR-181a overexpressing cell lines, was generously donated by Dr. Chen Z. Cheng (Stanford University). Mutations in the miR-181a seed sequence were generated using Change-IT Multiple Mutation Site-directed Mutagenesis kit (USB). Retrovirus was generated by co-transfection of the above constructs with packaging plasmids into Phx cells. A2780 cells were transduced and subsequently FACS-sorted for green fluorescent protein (GFP)-positivity, which is co-expressed on a single transcript with the miR-181a. The

pCDNA3.1-Smad7 construct was generously provided by Dr. Carl-Hendrik Heldin (Ludwig Institute for Cancer Research, Sweden). The Smad7 cDNA lacking the 3'UTR was excised out of the pCDNA3.1 vector backbone using BamH1 and Xho1 (NEB) and amplified by PCR; the purified cDNA was then ligated into the pBABE-puro vector backbone post-digestion with BamH1 and Sal1 (NEB). The newly generated pBABEpuro-Smad7 plasmid was then trasnfected into Phx cells as described above, and selection of positively transduced cells was accomplished using 2.5 μg/mL puromycin (Invitrogen).

microRNA sensor and decoy vectors.

The sensor construct was generated as previously described (44). A bidirectional lentiviral vector, which expresses GFP and mCherry as two distinct transcripts, was modified to contain four tandem copies of an imperfectly complementary target site for miR-181a. A2780 and SKOV3 cells were transduced with the miR-181a sensor and an empty control as described above. The FACS data were acquired using the BD LSR II machine and analyzed using FlowJo 8.8.7 software. The microRNA decoy vector utilized the tough decoy (TuD) configuration (18). Two semicomplementary target sites for miR-181a were cloned into a lentiviral vector, which also encoded a GFP reporter gene expressed from the PGK promoter. The vectors were produced and titered as previously described (40).

Clonogenecity Assay.

Cell survival was assessed through seeding 250 cells/well in a 6-well plate and were fixed in a 10% acetic acid/10% methanol (in diH2O) solution and stained with 1% crystal violet (in methanol) after 7 days of growth. Colonies were counted using ImageJ.

Cell migration assay.

Cell migration was determined by means of wound-healing assay and transwell migration assay. For the wound-healing assay, $4x10^5$ cells were seeded into six-well plates and were serum starved for 24h once they were fully confluent. A sterile 200 μl pipette tip was used to scratch the cells to form a wound. The cells were washed with PBS and cultured in serum-free medium. The assay was performed in complete media with SKOV3-derived cells. Migration of the cells to the wound was visualized with an inverted Nikon Eclipse TS100 phase-contrast microscope and measured using Nikon NIS-Element Basic Research v3.2 software. The transwell migration assay was performed in triplicate (Cell BioLabs, catalog no. CBA-100). 300,000 cells (in serum-free media) were plated into the upper chambers that comprised of a polycarbonate membrane (8 μM pore-size, ideal for epithelial cells) through which migratory cells would penetrate. The cells were incubated in 37°C for 24 hours and were subsequently harvested for quantification via a colorimetric absorbance reading (per Cell BioLabs protocol) at 560 nm. It is important to note that all non-migratory cells were removed from the upper chamber before assaying and quantifying the migratory cells on the bottom chamber.

Gene expression analysis using RNA-sequencing (RNA-seq) data.

Total RNA was extracted from two polyclonal pools of A2780 cells expressing exogenous miR-181a (p181a #1 and p181a #2) and an empty vector control expressing pBABE-GFP (pBABE). The Illumina RNASeq kit was used to prepare sequencing libraries. The method is as follows: 1 μg of high quality total RNA was incubated with oligo(dT) magnetic beads (SeraMag) in order to enrich for mRNA with poly-A tails. Eluted RNA was randomly cleaved by incubation at 94°C with a magnesium buffer; this yields ~200 nt fragments. The RNA is ethanol-precipitated and then reverse transcribed (Invitrogen SuperScript II). DNA polymerase is added to generate a second strand.

dsDNA after second strand synthesis contains ends with 5´ and 3´ overhangs, and these are filled in using T4 polymerase and T4 polynucleotide kinase resulting in a blunt-ended DNA molecule. Then a deoxyadenosine (dA) 5´ tail is added to DNA strands using the Klenow fragment (exo-). dsDNA adapters with 3´ thymidine overhangs are ligated to the dA-tailed library using T4 ligase. The library was then size selected on a 2% agarose gel, and amplified with 15 cycles of PCR (NEB Phusion polymerase). This procedure adds the sequences needed for binding to the Illumina flow cell and sequencing primer-binding sites. RNA-Seq libraries were sequenced using the Illumina HiSeq 2000 for a 100nt read length. Transcriptome raw reads from Illumina's GAIIx were mapped to the human reference genome (hg19). The coverage over the length of the gene is variable due to various biases inherent to the sequencing and sample preparation process. To avoid problems arising from this, we generated a density profile using windows of 50 bp sliding over the length of each gene, and the median of this density profile was picked as the representative coverage for the gene using an in-house mRNA-seq expression profile pipeline. The coverage is corrected using log-transformation and quantile normalization. Putative miRNA targets were predicted using TargetScan (http://www.targetscan.org) and miRConnect (http://mirconnect.org).

Smad7 3'UTR Reporter Assay.

The 3'UTR of Smad7 was obtained from Switgear Genomics. Renilla luciferase reporter plasmid (500 ng) and pGL3-control (100 ng for normalization) (Promega) were co-transfected with Lipofectamine 2000 (Invitrogen) into cell lines seeded in 12-well plates ($1x10^5$ cell/well). Cells were collected after 24h for assay using the Dual-Luciferase Reporter Assay System (Promega). All experiments were done in triplicate with data pooled from 3 independent experiments.

p3TP Luciferase-based Reporter Assay.

All A2780 cell lines (controls and p181a#1, #2) were plated at 50,000 per well and were serum-starved 6 hours pre-transfection. The firefly-based luciferase p3TP reporter construct (AddGene) at 900 ng with a renilla-based tkrl control construct at 150 ng, with Lipofectamine2000 (1.5μL/μg of plasmid). The cells were harvested 24 hours post-transfection; all p3TP-based firefly-luciferase readout values were normalized to the tkrl renilla values (FL/RL).

SBE4-luc Reporter Assay.

A reporter to detect TGF-β-signaling pathway activity was obtained from Addgene. For the transfection, $1x10^5$ cells were seeded 24h prior to co-transfection with pSBE4-luc and TKRL (Renilla Luciferase control). Recombinant TGF-β ligand (eBiosciences) was added 6h prior to harvest and the luciferase activity was determined using the Dual-Luciferase Reporter Assay System (Promega). All experiments were done in triplicate with data pooled from 3 independent experiments.

Immunoblotting.

Whole cell protein extracts were obtained with radio-immunoprecipitation assay buffer following standard protocols. The protein extracts were denatured and 40-50 μg of each sample were separated on 12% SDS PAGE gels and transferred to nitrocellulose membranes. After blocking with 5% non-fat milk (Labscientific, Inc) in TBS-Tween buffer, the membranes were probed with anti-E-cadherin (Santa Cruz), anti-N-cadherin (Santa Cruz), anti-Smad7 (Santa Cruz), anti-ACTR-IIA (Santa Cruz), anti-ACTR-IIB (Santa Cruz), anti-Actin (Santa Cruz), anti-Keratin 8 (Epitomics), anti-Col3A1 (Abcam), anti-Smad2 (Cell Signaling), anti-PSmad2 (Cell Signaling), anti-Smad3 (Cell Signaling),

anti-P-Smad3 (Cell Signaling), and anti-Fibronectin (BD Transduction Lab). Membranes were exposed using ECL (Roche) method following manufacturer's instructions.

Immunohistochemical staining for pSmad2 in human ovarian tumor tissue samples.

Paraffin-embedded ovarian tumor tissue samples were deparaffinized in Histoclear and rehydrated in successive ethanol washes. Endogenous peroxidase was quenched using 10% 30%-Hydrogen peroxide in methanol for 15 minutes. Antigen retrieval was achieved at 124 degrees Celsius for 5 minutes and the tissue were subsequently incubated in normal goat serum (in PBS) for 1 hr at room temperature. The tissue was incubated in primary anti-pSmad2 antibody (Cell Signaling) overnight in 4 degrees Celsius. Incubation in secondary antibody (goat-derived anti-rabbit IgG) was followed by addition of horseradish peroxidase (Invitrogen). DAB (Vectashield) was added for 5 minutes; counterstaining was achieved in hematoxylin. Subsequently, the tissue were dehydrated in successive ethanol washes and deparaffinized in Histoclear before mounting with Permount. The diluent used for this protocol was 5% BSA in TBS-Tween. Overall immune scores were calculated using the Allred scoring system (Allred et al., 1998). Specifically, the immune score was determined by adding the intensity score 0-3 (0=no immunoreactivity, 1=weak positive staining, 2=moderate positive staining and 3=strong positive staining) and extent score 0-5 (0=0%, 1=1-25%, 2=26-50%, 3=51-75% and 4=76-100%) ranged from 0-7 and the median score for the cases was 2. After dichotomizing the group at that median kaplan-meier analysis was performed and Logrank test was utilized to assess the statistical significance.

In vivo studies.

All *in vivo* experiments were performed according to approved protocols from the Animal Research Committee at the Mount Sinai School of Medicine. A2780 pBABE and p181a #1 cells ($2x10^6$) were injected intraperitoneally in 6- to 8-week old female SCID mice. All mice were sacrificed after 3 weeks to compare relative tumor burden. RNA from tumor tissue was extracted as described above.

Statistical analysis.

Unless otherwise noted, data are presented as mean ± SD from three-independent experiments, and Student's *t*-test (two-tailed) was used to compare two groups ($P<0.05$ was considered significant) for independent samples.

ACKNOWLEDGEMENTS

The authors thank Robert Chong for pSBE4-luc vector, Dr. Paul Modrich for the A2780 cell lines, Dr. Chen Z. Cheng and Dr. Carl-Hendrik Heldin for the expression vectors, Dr. William Schmeimann for the p3TP vector, and Dr. Scott Howell for his help with immunofluorescence and microscopy work and members of Dr. Goutham Narla laboratory for helpful discussions. RNA-Sequencing was performed at the Institute for Genomics and Multiscale Biology, Mount Sinai School of Medicine. We thank Vyom Mehta for performing the RNA-Seq sample preparation. This work was supported by grants from the Ovarian Cancer Research Program CDMRP (W81XWH-11-1-0609), Department of Defense (AD), Ovarian Cancer Research Fund Liz Tilberis Scholar (AD), and the Young Scientist Cancer Research Fund at Mount Sinai School of Medicine (AD, GN). We acknowledge the generous contributions of the Nerina and Mario Mattioli Foundation, ACTO, and the Italian Association for Cancer Research (IG11673).

REFERENCES

1. R. Siegel, E. Ward, O. Brawley, A. Jemal, Cancer statistics. Cancer J Clin. **61***,* 212-236 (2011).

2. J.D. Seidman, R.A. Soslow, R. Vang, J.J. Berman, M.H. Stoler, M.E. Sherman, E. Olivia, A. Kajdacsy-Balla, D.M. Berman, L.J. Copeland, Borderline ovarian tumors: diverse contemporary viewpoints on terminology and diagnostic criteria with illustrative images. Hum Pathol. **35***,* 918-933 (2004).

3. M.S. Kumar, J. Lu, K.L. Mercer, T.R. Golub, T. Jacks, Impaired microRNA processing enhances cellular transformation and tumorigenesis. Nat Genet. **39***,* 673-677 (2007).

4. D. Yang, Y. Sun, H. Limei, H. Zheng, P. Ji, C.V. Pecot, Y. Zhao, S. Reynolds, H. Cheng, R. Rupaimoole, et al., Intregrated Analyses Identify a Master MicroRNA Regulatory Network for the Mesenchymal Subtype in Serous Ovarian Cancer. Cancer Cell. **23**, 186-199 (2013).

5. B. Mateescu, L. Batista, M. Cardon, T. Gruosso, Y. de Feraudy, O. Mariani, A. Nicolas, J.P. Meyniel, P. Cottu, X. Sastre-Garau, et al, miR-141 and miR-200a act on ovarian tumorigenesis by controlling oxidative stress response. Nat Med. **17***,* 1627-1635 (2011).

6. M.V. Iorio, R. Visone, G. Di Leva, V. Donati, F. Petrocca, P. Casalini, C. Taccioli, S. Volinia, C.G. Liu, H. Alder, et al*.,* microRNA signatures in human ovarian cancer. Cancer Res. **67***,* 8699-8707 (2007).

7. E.J. Nam, H. Yoon, S.W. Kim, H. Kim, Y.T. Kim, J.H. Kim, J.W. Kim, S. Kim, MicroRNA expression profiles in serous ovarian carcinoma. Clin Cancer Res. **14***,* 2690-2695 (2008).

8. N. Yang, S. Kaur, S. Volinia, J. Greshock, H. Lassus, K. Hasegawa, S. Liang, A. Leminen, S. Deng, L. Smith et al., MicroRNA microarray identifies Let-7i as a novel biomarker anti-therapeutic target in human epithelial ovarian cancer. Cancer Res. **68***,* 10307-10314 (2008).

9. N. Dahiya, P.J. Morin, MicroRNAs in ovarian carcinomas. Endocr Relat Cancer. **17***,* F77-89 (2010).

10. N. Dahiya, C.A. Sherman-Baust, T.L. Wang, B. Davidson, IeM. Shih, Y. Zhang, W. Wood 3rd, K.G. Becker, P.J. Morin, MicroRNA expression and identification of putative miRNA targets in ovarian cancer. PLoS One. **18***,* e2436 (2008).

11. A. Sherman, L. Hu, C. Melton, D. Kapp, J. Chan, Differential microRNA expression in cis-platinum-resistant versus -sensitive ovarian cancer cell lines. Gynecologic Oncology. **120**, S48 (2011).

12. X. Li, J. Zhang, L. Gao, S. McClellan, M.A. Finan, T.W. Butler, L.B. Owen, G.A. Piazza, Y. Xi, MiR-181 mediates cell differentiation by interrupting the Lin28 and let-7 feedback circuit. Cell Death Differ. **19***,* 378-386 (2012).

13. C.C. Yang, P.S. Hung, P.W. Wang, C.J. Liu, T.H. Chu, H.W. Cheng, S.C. Lin, miR-181 as a putative biomarker for lymph-node metastasis of oral squamous cell carcinoma. J Oral Pathol Med. **40***,* 397-404 (2011).

14. J. Ji, T. Yamashita, A. Budhu, M. Forgues, H.L. Jia, C. Li, C. Deng, E. Wauthier, L.M. Reid, Q.H. Ye, et al., Identification of microRNA-181 by genome-wide screening as a critical player in EpCAM-positive hepatic cancer stem cells. Hepatology. **50***,* 472- 480 (2009).

15. D. Iliopoulos, S.A. Jaeger, H.A. Hirsch, M.L. Bulyk, K. Struhl, STAT3 activation of miR-21 and miR-181b-1 via PTEN and CYLD are part of the epigenetic switch linking inflammation to cancer. Molecular Cell. **39**, 439-506 (2010).

16. T.W. Corson, et al Kif14 is a candidate oncogene in the 1q minimal region of genomic gain in multiple cancers. Oncogene **24**, 4741-4753 (2005).

17. B.L. Therlault, N.W. Nachtigal, Human ovarian cancer cell morphology, motility, and proliferation are differentially influenced by autocrine TGFβ superfamily signalling. Cancer Lett. **313**, 108-121 (2011).

18. R. Navon, H. Wang, I. Steinfeld, A. Tsalenko, A. Ben-Dor, Z. Yakhini, Novel Rank-Based Statistical Methods Reveal MicroRNAs with Differential Expression in Multiple Cancer Types. PLoS One. 11, e8003 (2009).

19. T. Haraguchi, Y. Ozaki, H. Iba, Vectors expressing efficient RNA decoys achieve long-term suppression of specific microRNA activity in mammalian cells. Nuc Acids Res. **6**, e43 (2009).

20. A. Baccarini, H. Chauhan, T.J. Gardner, A.D. Jayaprakash, R. Sachidanandam, B.D. Brown, Kinetic analysis reveals the fate of a microRNA following target regulation in mammalian cells. Curr Biol. **21**, 369-376 (2011).

21. H. Guo, N. Ingolia, J. Weissman, D. Bartel, Mammalian microRNAs predominantly act to decrease target mRNA levels. Nature **466**, 835–840 (2010).

22. M. Zeisberg, R. Kalluri, The role of epithelial-to-mesenchymal transition in renal fibrosis. J Mol Med (Berl). **82***,* 175-181 (2004).

23. K. Pardali, A. Moustakas, Actions of TGF-beta as tumor suppressor and pro-metastatic factor in human cancer. Biochim Biophys Acta. **1**, 21-62 (2007).

24. J. Helleman, M.P. Jansen, C. Burger, M.E. van der Burg, E.M. Berns, Integrated genomics of chemotherapy resistant ovarian cancer: a role for extracellular matrix, TGFbeta and regulating microRNAs. Int J Bioche Cell Biol. **42***,* 25-30 (2010).

25. D.C. Allred, J.M. Harvey, M. Berardo, G.M. Clark, Prognostic and predictive factors in breast cancer by immunohistochemical analysis. Mod Pathol. **11***,* 155-68 (1998).

26. S. Marchini, R. Fruscio, L. Clivio, L. Beltrame, L. Porcu, I.F. Nerini, D. Cavalieri, G. Chiorino, G. Cattoretti, C. Mangioni C, et al., Resistance to platinum-based chemotherapy is associated with epithelial to mesenchymal transition in epithelial ovarian cancer. European Journal of Cancer, **10,** 1016/j.ejca. (2012).

27. D. Bell, A. Berchuck, M. Birrer, J. Chien, D.W. Cramer, F. Dao, R. Dhir, P. DiSaia, H. Gabra, P. Glenn, et al., The Cancer Genome Atlas. Integrated genomic analyses of ovarian carcinoma. Nature. **474***,* 609-615 (2011).

28. R.L. Baldwin, H. Tran, B.Y. Karlan, Loss of c-myc repression coincides with ovarian cancer resistance to transforming growth factor beta growth arrest independent of transforming growth factor beta/Smad signaling. Cancer Res. **63**, 1413-1419 (2003).

29. S. Yamamura, N. Matsumura, M. Mandai, Z. Huang, T. Oura, T. Baba, J. Hamanishi, K. Yamaguchi, H.S. Kang, T. Okamoto, et al*.,* The activated transforming growth factor-beta signaling pathway in peritoneal metastases is a potential therapeutic target in ovarian cancer. Int J Cancer. **130***,* 20-28 (2012).

30. T.V. Do, L.A. Kubba, H. Du, C.D. Sturgis, T.K. Woodruff, Transforming growth factor-beta1, transforming growth factor-beta2, and transforming growth factor-beta3 enhance ovarian cancer metastatic potential by inducing a Smad3-dependent epithelial-to-mesenchymal transition. Mol Cancer Res. **6***,* 695-705 (2008).

31. L. Cao, M. Shao, J. Schilder, T. Guise, K.S. Mohammad, D. Matei, Tissue transglutaminase links TGF-β , epithelial to mesenchymal transition and stem cell phenotype in ovarian cancer. Oncogene. **31**, 2521-34 (2012).

32. R. Henriksen, A. Gobl, E. Wilander, K. Oberg, K. Miyazono, K. Funa, Expression and prognostic significance of TGF-beta isotypes, latent TGF-beta 1 binding protein, TGF-beta type I and type II receptors, and endoglin in normal ovary and ovarian neoplasms. Lab Invest. **73**, 213-20 (1995).

33. A.L. Smith, R. Iwanaga, D.J. Drasin, D.S. Micalizzi, R.L. Vartuli, A.C. Tan, H.L. Ford, The miR-106b-25 cluster targets Smad7, activates TGF-beta signaling, and induces EMT and tumor initiating cell characteristics downstream of Six1 in human breast cancer. Oncogene, **31,** 5162–5171 (2012).

34. L. Ma, F. Reinhardt, E. Pan, J. Soutschek, B. Bhat, E.G. Marcusson, J. Teruya-Feldstein, G.W. Bell, R.A. Weinberg, Therapeutic silencing of miR-10b inhibits metastasis in a mouse mammary tumor model. Nature Biotechnology. **28**, 341–347 (2010).

35. P.A. Gregory, A.G. Bert, E.L. Paterson, S.C. Barry, A. Tsykin, G. Farshid, M.A. Vadas, Y. Khew-Goodall, G.J. Goodall, The miR-200 family and miR-205 regulate epithelial to mesenchymal transition by targeting ZEB1 and SIP1. Nature Cell Biology. **10**, 593 - 601 (2008).

36. C. Faleiro-Rodrigues, I. Macedo-Pinto, D. Pereira, C.S. Lopes, Prognostic value of E-cadherin immunoexpression in patients with primary ovarian carcinomas. Ann Oncol. **15**,1535-42 (2004).

37. E Darai, J-Y Scoazec, F Walker-Combrouze et al. Expression of cadherins in benign, borderline, and malignant ovarian epithelial tumors. Hum Pathol **28**, 922–928 (1997).

38. L. Quattrocchi, A.R. Green, S. Martin, L. Durrant, S. Deen, The cadherin switch in ovarian high-grade serous carcinoma is associated with disease progression. Virchows Arch. **459**, 21-9 (2011).

39. J. Lu, G. Getz, E.A. Miska, E. Alvarez-Saavedra, J. Lamb, D. Peck, A. Sweet-Cordero, B.L. Ebert, R.H. Mak, A.A. Ferrando, J.R. Downing, T. Jacks, H.R. Horvitz, T.R. Golub, MicroRNA expression profiles classify human cancers. Nature. 435, 834-8 (2005).

40. A. Baccarini, B.D. Brown, Monitoring microRNA activity and validating microRNA targets by reporter-based approaches. Methods Mol Biol. **667***,* 215-233 (2010).

TABLES

Table 1

Gene symbol	RefSeq	Fold Change
Genes downregulated during EMT		
KRT18*	NM_199187	-5.80
NUDT13	NM_015901	-4.97
OCLN	NM_002538	-2.16
KRT8*	NM_002273	-2.02
RGS2	NM_002923	-1.21
Genes upregulated during EMT		
CDH2*	NM_001792	7.3
TIMP1	NM_003254	4.6
COL3A1*	NM_000090	4.0
TGFB2	NM_001135599	4.0
SNAI2*	NM_003068	3.2
ITGAV	NM_001145000	2.7
SPARC	NM_003118	2.7
COL5A2	NM_000393	2.2
ITGA5	NM_002205	2.1
TGFBR1	NM_001130916	2.1
TGFBR1	NM_004612	2.0
VIM*	NM_003380	2.0
SNAI3*	NM_178310	2.0
COL1A2	NM_000089	1.8
TMEFF1	NM_003692	1.5
STEAP1	NM_012449	1.4

Table 2

Immune Score	PFI<6 months	PFI>6 months
<2	11	17
≥2	14	4
N=	25	21

Fisher Exact test (*P=0.016)

FIGURE LEGENDS

Fig. 1. miR-181a levels are associated poor outcome and shorter time to recurrence in advanced epithelial ovarian cancer.

(A) Kaplan-Meier curves for progression-free survival (PFS) and overall survival (OS) in a cohort of patients (N=53) with stage III primary ovarian serous adenocarcinoma according to relative expression levels of miR-181a. Relative expression levels were dichotomized at the median. Median PFS for patients with low miR-181a expression was 55.9 months compared to 7.1 months in patients with high expression levels (*P*=0.002, OR= 7.8, 95% CI: 7.2-8.4). Median survival according to the miR-181a status also shows divergent Kaplan-Meier curves which was statistically significant (log rank statistical test *P*=0.002 for miR-181a). **(B)** Increased relative levels of miR-181a in patient tumor specimens with short progression free survival (PFS<6 months) compared to the levels in patients with PFS>6 months (*P*=0.01) as measured by Taqman qRT-PCR. Error bars show mean ± SD. Taqman qRT-PCR data was also normalized to miR-16. * *P*<0.05, ** *P*<0.01, *** *P*<0.001. **(C)** qRT-PCR analysis showing relative miR-181a expression levels in a panel of ovarian cancer cell lines and in two polyclonal pools of A2780 cells expressing exogenous miR- 181a (p181a #1 and p181a #2). miRNA expression normalized to U6. **(D)** Phase contrast microscopic images of miR-181a-overexpressing cells display morphological changes indicative of EMT. **(E)** Changes in the expression of epithelial and mesenchymal markers in miR-181a-overexpressing cells as measured by qRT-PCR and western blotting. **(F)** Clonogenic assay to assess the effects of miR-181a on cellular survival in miR-181a-overexpressing cells **(G)** and their response to cisplatin. Cells were plated in a 6-well plate and were treated every 3 days (d); colonies were counted after 8d. **(H)** Wound healing assay to assess effects on cellular motility. miR-181a-overexpressing cells and control cell lines ($4x10^5$) were plated in a 6-well plate.

Once the cells reached 100% confluency, these cells were serum-starved for 12 hours (h) and the scraped wound was measured every 12h. **(I)** Additional assessment of the migratory potential in 181a overexpressing A2780 cells. A traditional transwell migration assay was utilized to assess motility of overexpressing cells across a polycarbonate membrane; p181a#1 and #2 cells exhibited between a 50% increase (P>0.01) and nearly 3-fold increase (P>0.0001) in migration. A colorimetric assay was used to quantitate the number of migratory cells. **(J)** Total tumor burden in pBABE vs. p181a mice at 3 weeks post-intraperitoneal injection (left panel). Fisher's Exact test correlating the incidence of intraperitoneal (IP) nodules with **(K)** the enhanced expression of miR-181a **(L)** Fold change in expression of epithelial and mesenchymal molecular markers *in vivo*. Error bars show mean ± SD. * P<0.05, ** P<0.01, *** P<0.001.

Fig. 2. Stable inhibition of miR-181a results in reduced cellular motility and survival.

(A) Fold change of miR-181a expression levels in SKOV3 cell line stably transduced with miR-181a tough decoy vector and a control decoy vector for stable knockdown. **(B)** Monitoring functional activity of miR-181a in SKOV3 using sensor vectors as described above (Fig. 1) via mean fluorescent intensity measurements using flow cytometry. **(C)** Morphological changes indicate the reversion of miR-181a-induced EMT upon functional inhibition as confirmed by western blotting for epithelial (E-cadherin) and mesenchymal markers (Col3A1 and N-cadherin). **(D)** Clonogenic assay to assess cellular survival in miR-181a decoy cells. Control decoy cells show >8-fold higher number of colonies in formation when compared to the miR-181a decoy cells (P>0.0001). **(E)** Wound healing assay to evaluate cell motility in SKOV3 decoy cell lines. Cells ($4x10^5$) were plated in a

6-well plated; a scratch was made when cells reached 100% confluency. Error bars show mean ± SD. * P<0.05, ** P<0.01, *** P<0.001.

Fig. 3. miR-181a overexpression results in a significant enrichment of TGF-β signaling associated genes and is a novel modulator of the TGF-β signaling pathway.

(A) Global Canonical Pathway Analysis. RNA-sequencing datasets from A2780 pBABE and p181a #1 cell lines were analyzed using the Ingenuity Pathways Analysis software (Ingenuity® Systems, http://www.ingenuity.com). Significance is expressed as a p-value calculated using the right-tailed Fisher's Exact test. **(B)** Western blotting for the TGF-β Receptor proteins, Activin Receptor proteins and Smad proteins assessing TGF-β signaling pathway activity in miR-181a-overexpressing and control cells. **(C)** TGF-β transcriptional activity was assessed using both the firefly luciferase-based p3TP-lux (left) and SBE4 (right) reporter constructs. miR-181a overexpressing cells exhibit up to 7-8-fold higher p3TP reporter activity *(P*>0.0001); and SBE4 reporter activity was increased ~2-fold in both miR-181a stable cell lines *(P*>0.0001). Firefly luciferase readouts were normalized to renilla values as determined by TKRL co-transfection. **(D)** Decreased responsiveness to TGF-β ligand in SKOV3 cells transduced with miR- 181a decoy compared to the control decoy as measured by relative luciferase activity using Smad-binding element luciferase construct as described above. **(E)** The TGF-β RI inhibitor, SB431542, blunted miR-181a activation of the TGF-β signaling as measured by phospho-Smad2. **(F)** Immunohistochemical assessment of pSmad2 expression in advanced EOC patients. Immune scores were established using the Allred scoring system based on both the extent of staining and intensity of expression, which ranged from 0-7. **(G)** Kaplan-Meier curves derived from dichotomizing pSmad2 expression at

the median based on the immune scores show significant differences in progression-free survival (PFS) and overall survival (OS). The median PFS for patients with low pSmad2 (I.S.≤2) expression was 53.1 months compared to 6.7 months in patients with high pSmad2 expression (I.S.≥2) (*P*=0.03, OR= 7.9, 95% CI: 7.4-8.5). Median overall survival was 72.8 months in low pSmad2 expressing patients and 25.5 months in high pSmad2 expressing patients (*P*=0.05, OR= 2.9, 95% CI: 2.3-3.4). **(H)** Kaplan-Meier analysis revealed that combining the status of both miR-181a and pSMAD2 expression had a highly significant difference in progression-free interval (PFI) and overall survival (OS) compared to assessing these survival outcomes for each biomarker alone. Patients with tumors that had both low miR-181a and pSMAD2 expression had a median PFI of 123 months (****P*=0.0007, OR 18.7; 95% CI: 9.2 to 37.8). Similarly, in patients with tumors that had both low miR-181a and pSMAD2 expression the median PFI was 132.2 months (****P*=0.0006, OR 5.8; 95% CI: 2.6 to 12.8).

Fig. 4. miR-181a expression analysis in a second clinical cohort.

(A) Box plot diagrams showing the expression analysis of miR-181a in a second clinical cohort of patient matched tumor specimens from **PS-O**, primary surgery, ovary (naïve to chemotherapy) and **SCR,** secondary surgery (after tumor has recurred and after two lines of chemotherapy). Within each box the horizontal line indicates the median. The top edge of the boxes represents the 75^{th} percentile, the bottom edge the 25^{th} percentile (note the log scale on the ordinate). The range is shown as a vertical line ending above and below the 75^{th} and 25^{th} percentile values, respectively. Individual dots represent the outliers. **(B)** Table summarizing the median and inter-quantile range (IQ-range) of fluorescent intensity normalized values for miR-181a in the validation set. All data are 10^4 transformed.). Group A and B represent the cohort of tumors with and without EMT signature, respectively as reported (Marchini et al. 2012). **R**, is the ratio between SCR

and PS-O. ***p*** <0.05 according to Wilcoxon matched-pairs signed rank test. *,<0.05; **, <0.01; ***, <0.001.

Fig. 5. Smad7 is a novel target of miR-181a.

(A) TGF-β -related genes that are putative miR-181a targets as predicted by TargetScan and miRConnect analysis. Smad7 is downregulated by >30 fold with exogenous miR-181a expression. **(B)** Conservation of the miR-181a-targeting sites in the Smad7 3'UTR and the miR-181a mutant sequence that abrogates miR-181a binding to target mRNA. **(C)** A Smad7 3'UTR renilla luciferase reporter plasmid was transiently co-transfected into all the A2780 overexpression stables along with a firefly luciferase reporter (pGL3 control) for normalization. Luciferase activities (RL/FL) were measured after 24h post-transfection. The data displays the means +/- SD of three separate transfections (data shown as the relative ratio of RL activity to FL activity). **(D)** Endogenous Smad7 mRNA expression as assessed by qRT-PCR in miR-181a-overexpressing and control cells. **(E)** Relative Smad7 mRNA expression in tumor tissue extracted from athymic mice 3-weeks post-intraperitoneal injection of miR-181a or control cells. **(F)** Analysis of the matched primary and recurrent ovarian tumors revealed a significant negative correlation (r =-0.96, P < 0.0001) between miR-181a expression and Smad7 expression, **G)** Smad7 3'UTR luciferase analysis in the SKOV3 ovarian cancer cell lines expressing miR-181a or control decoy. **(H)** Smad7 expression in SKOV3 cell lines with stable miR-181a inhibition as measured by real-time PCR and western blot. * *P*<0.05, ** *P*<0.01, *** *P*<0.001.

Fig. 6. Smad7 re-expression attenuates the miR-181a driven phenotypes. **(A)** Phase contrast microscopy images of A2780 cells stably overexpressing miR-181a or pBABE (control) in the presence and absence of Smad7 reconstitution. **(B)** qRT-PCR analysis showing Smad7, epithelial and mesenchymal marker gene expression. **(C)** Epithelial and mesenchymal marker expression in the Smad7 rescue stable cell lines as measured by western blotting. **(D)** Colony formation assays to assess attenuation of miR-181a-mediated pro-survival phenotype in A2780 cells overexpressing Smad7 and pBABE' control. **(E)** TGF-β signaling pathway activity as measured by a TGF-β responsive firefly luciferase reporter construct (SBE4-luc) as described above. Error bars show mean ± SD. * P<0.05, ** P<0.01, *** P<0.001.

Table 1. Enhanced miR-181a expression induces global changes in gene expression consistent with TGF-β mediated EMT. Exogenous miR-181a expression leads to differential transcriptomic changes of EMT markers, such as downregulation of Keratin 8/18, NUDT13, and others as well as upregulation of Col3A1.

Table 2. pSmad2 expression in advanced ovarian cancer patients negatively correlates with progression-free interval.

Figure 1

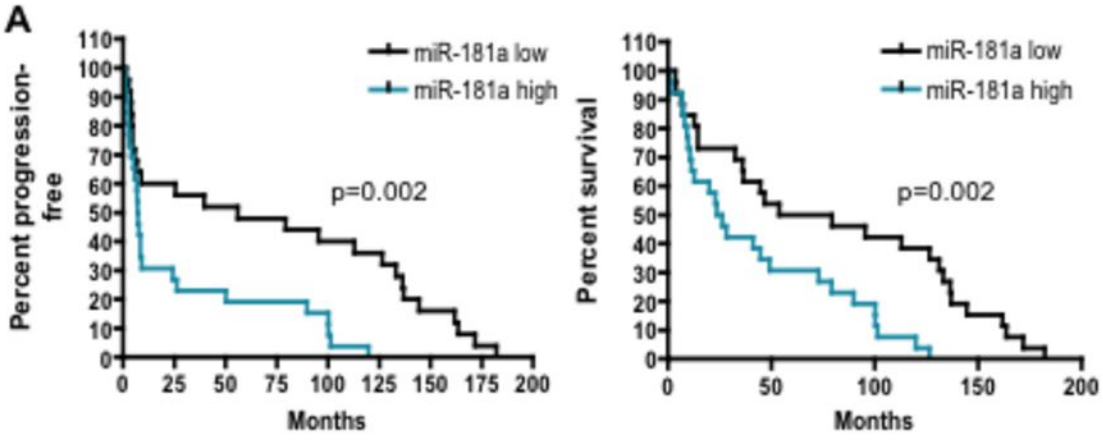

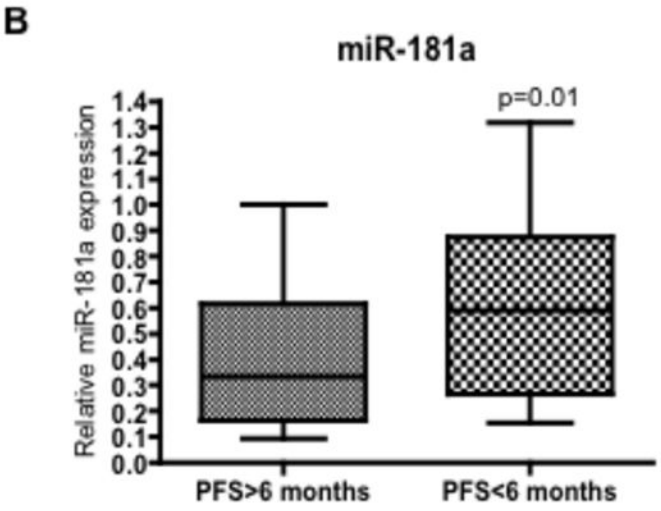

	miR-181a low	miR-181a high
Median PFS	55.9	7.1
**P=0.002, OR 7.8; 95% CI: 7.2 to 8.4		
Median survival	66.6	24.9
**P=0.002, OR 2.7; 95% CI: 2.1 to 3.3		

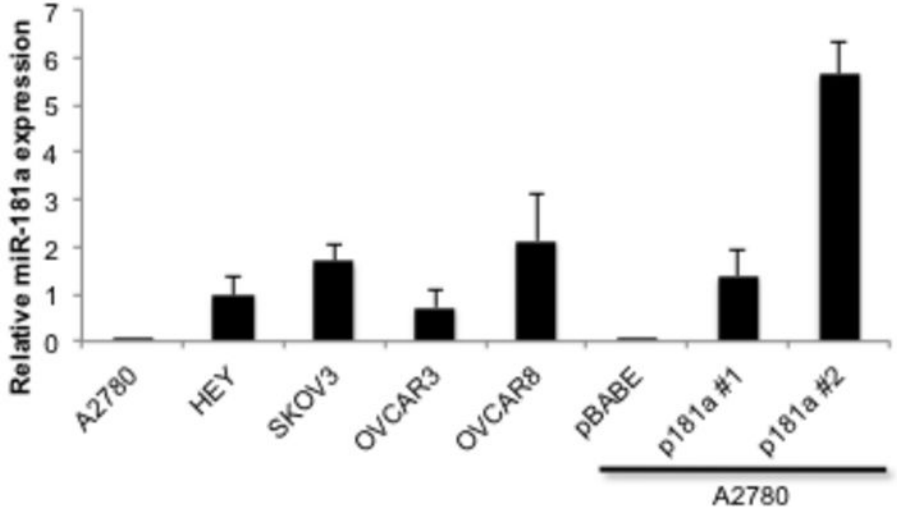

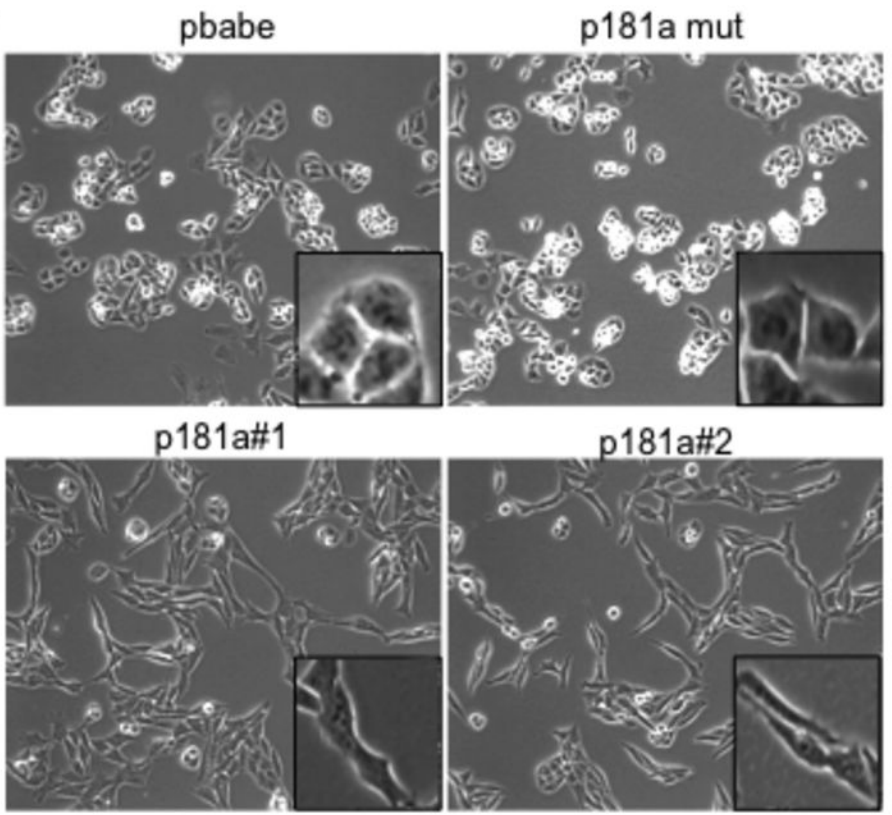

Figure 1

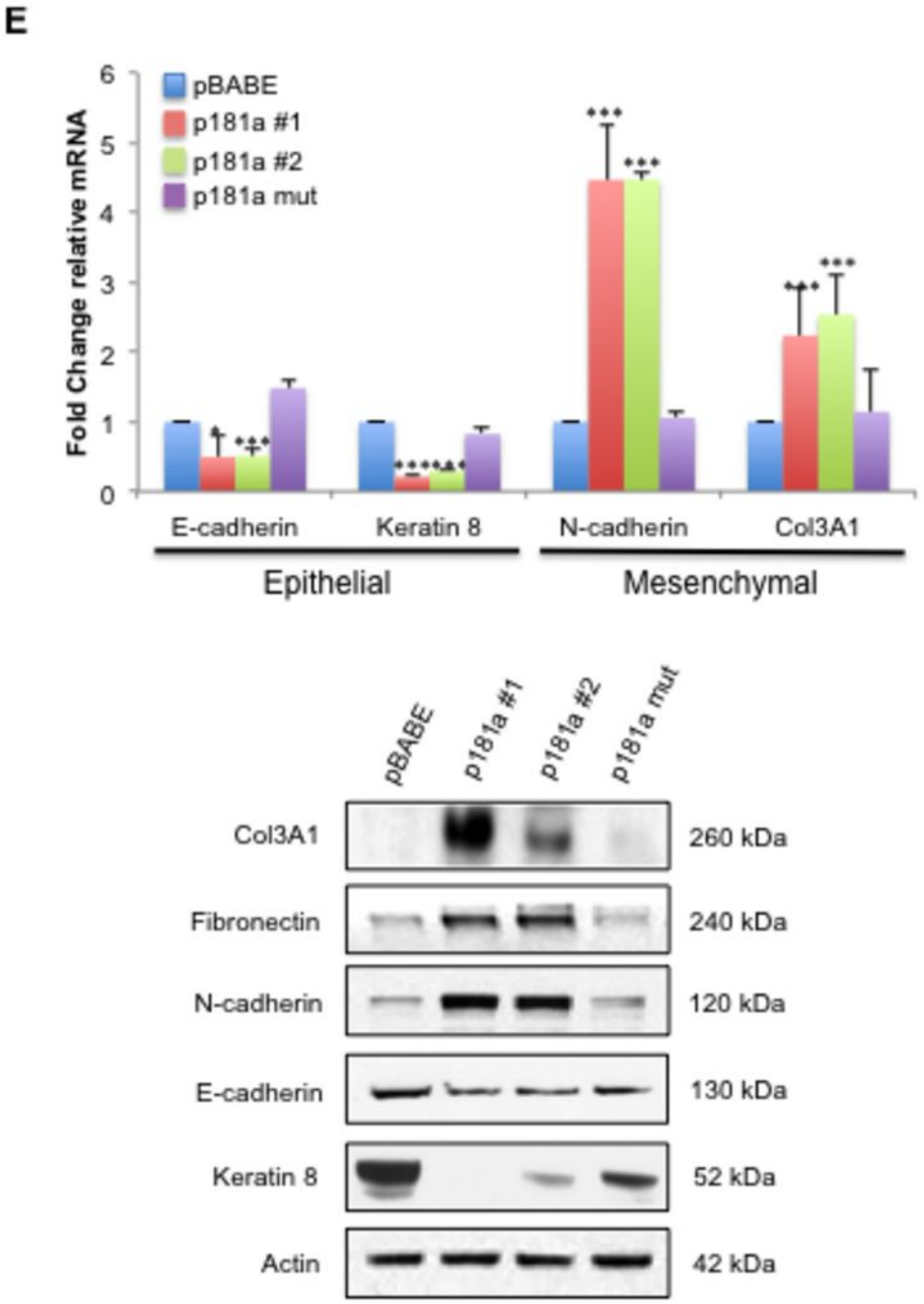
E
pBABE
p181a #1
p181a #2
p181a mut
Fold Change relative mRNA
E-cadherin
Keratin 8
N-cadherin
Col3A1
Epithelial
Mesenchymal
pBABE
p181a #1
p181a #2
p181a mut
Col3A1
260 kDa
Fibronectin
240 kDa
N-cadherin
120 kDa
E-cadherin
130 kDa
Keratin 8
52 kDa
Actin
42 kDa

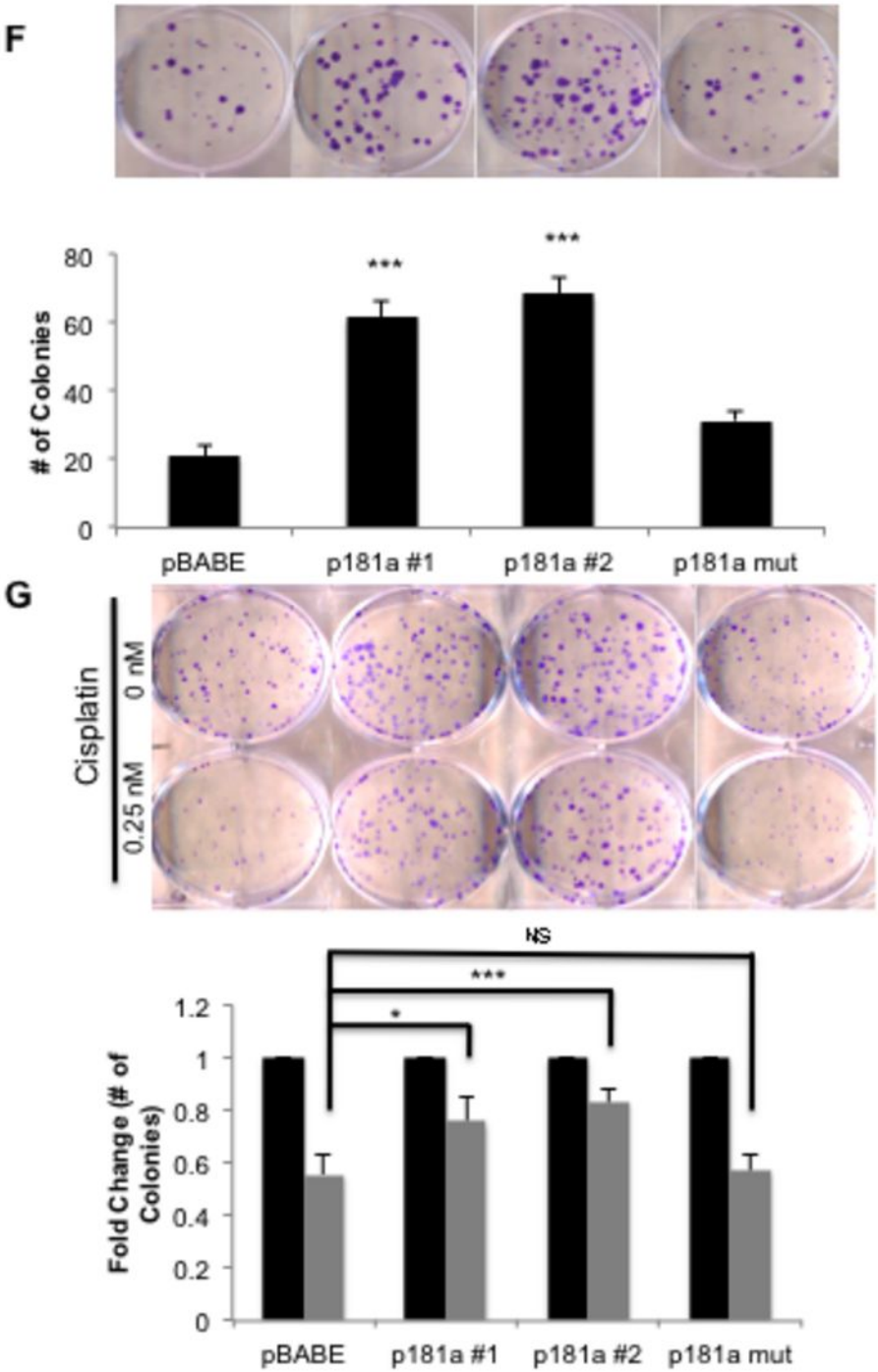
F
# of Colonies
pBABE
p181a #1
p181a #2
p181a mut
G
Cisplatin
0 nM
0.25 nM
NS
Fold Change (# of Colonies)
pBABE
p181a #1
p181a #2
p181a mut

Figure 1

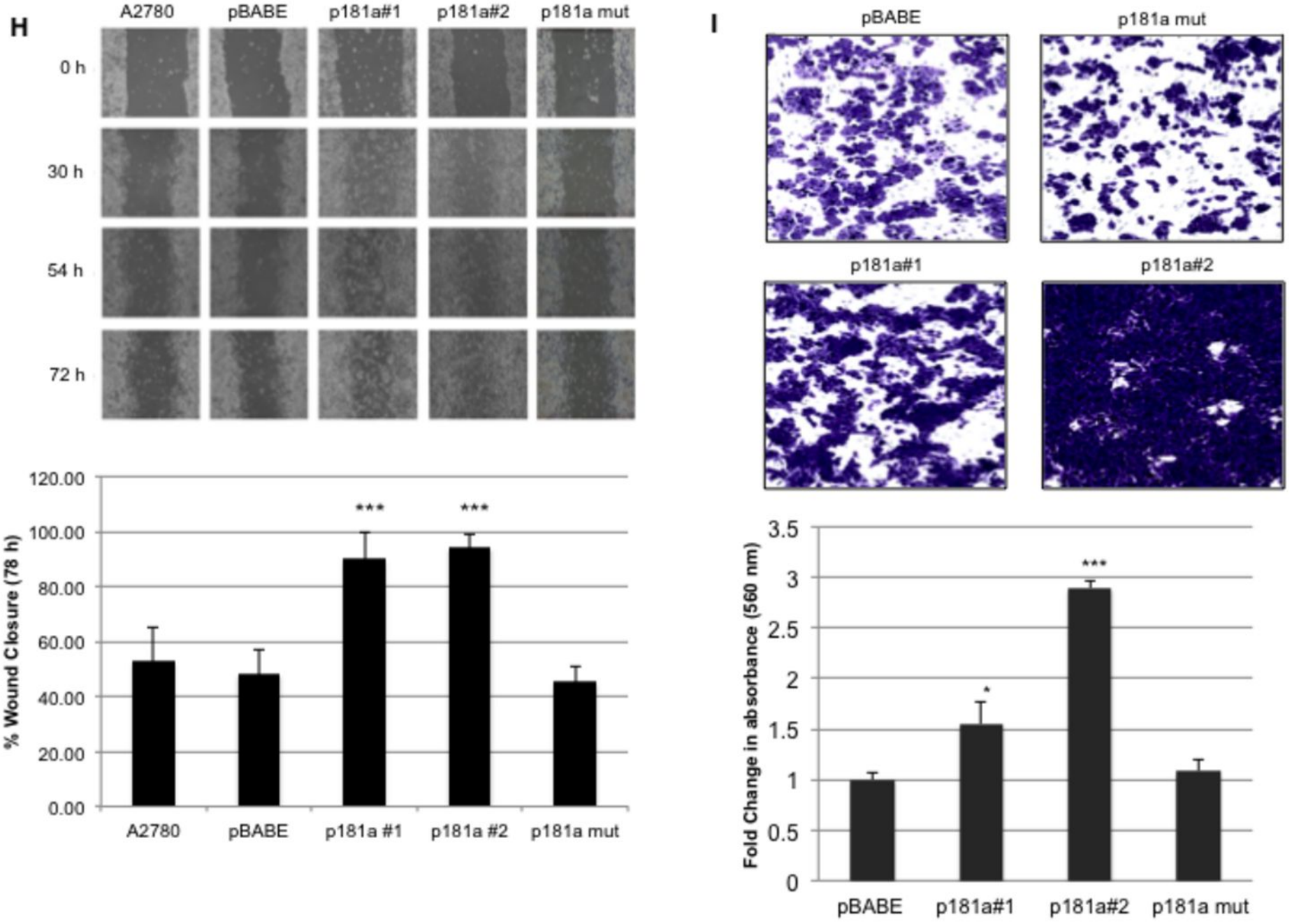
H
A2780
pBABE
p181a#1
p181a#2
p181a mut
0 h
30 h
54 h
72 h
% Wound Closure (78 h)
120.00
100.00
80.00
60.00
40.00
20.00
0.00
***
***
A2780
pBABE
p181a #1
p181a #2
p181a mut
I
pBABE
p181a mut
p181a#1
p181a#2
Fold Change in absorbance (560 nm)
3.5
3
2.5
2
1.5
1
0.5
0
*
***
pBABE
p181a#1
p181a#2
p181a mut

Figure 1

J

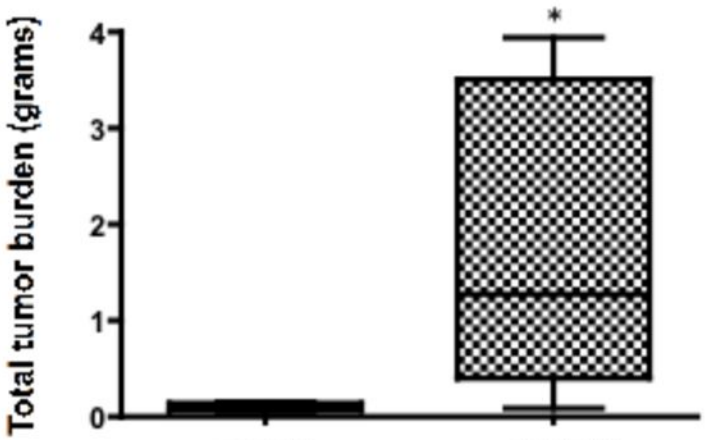

	No IP nodules	IP nodules
p181a #1	1	6 **
pBABE	5	0

Fisher's Exact test, *P*=0.01
OR: 47.67; 95% CI: 1.6-1424

K

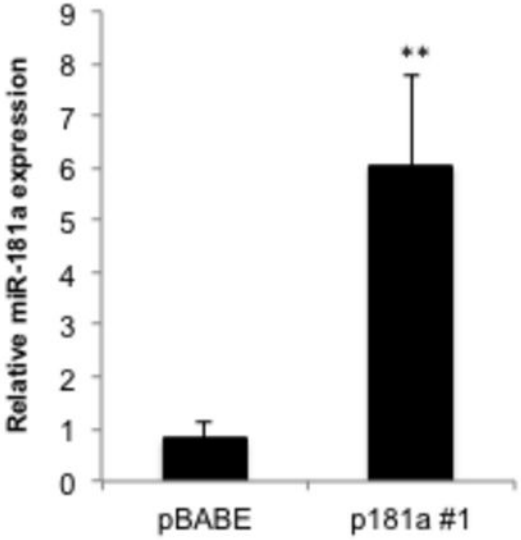

L

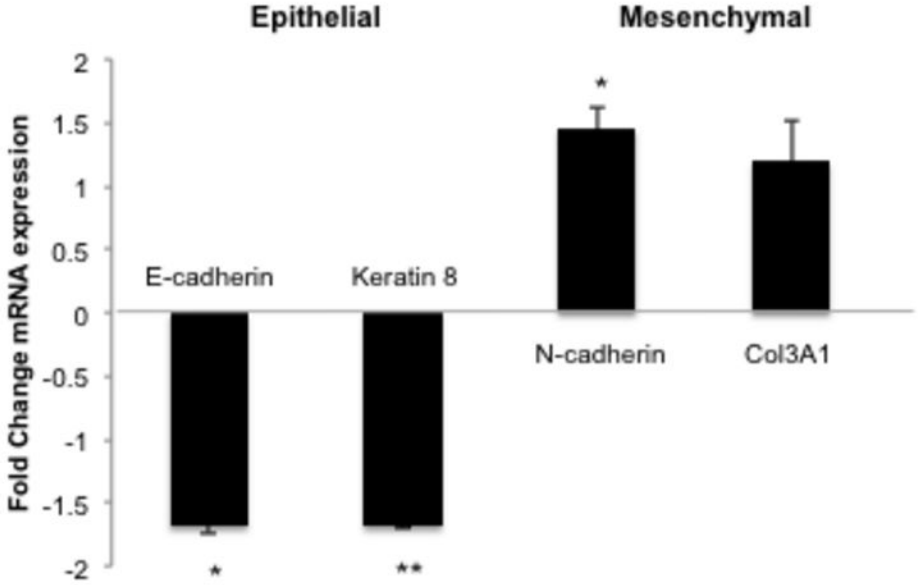

Figure 2

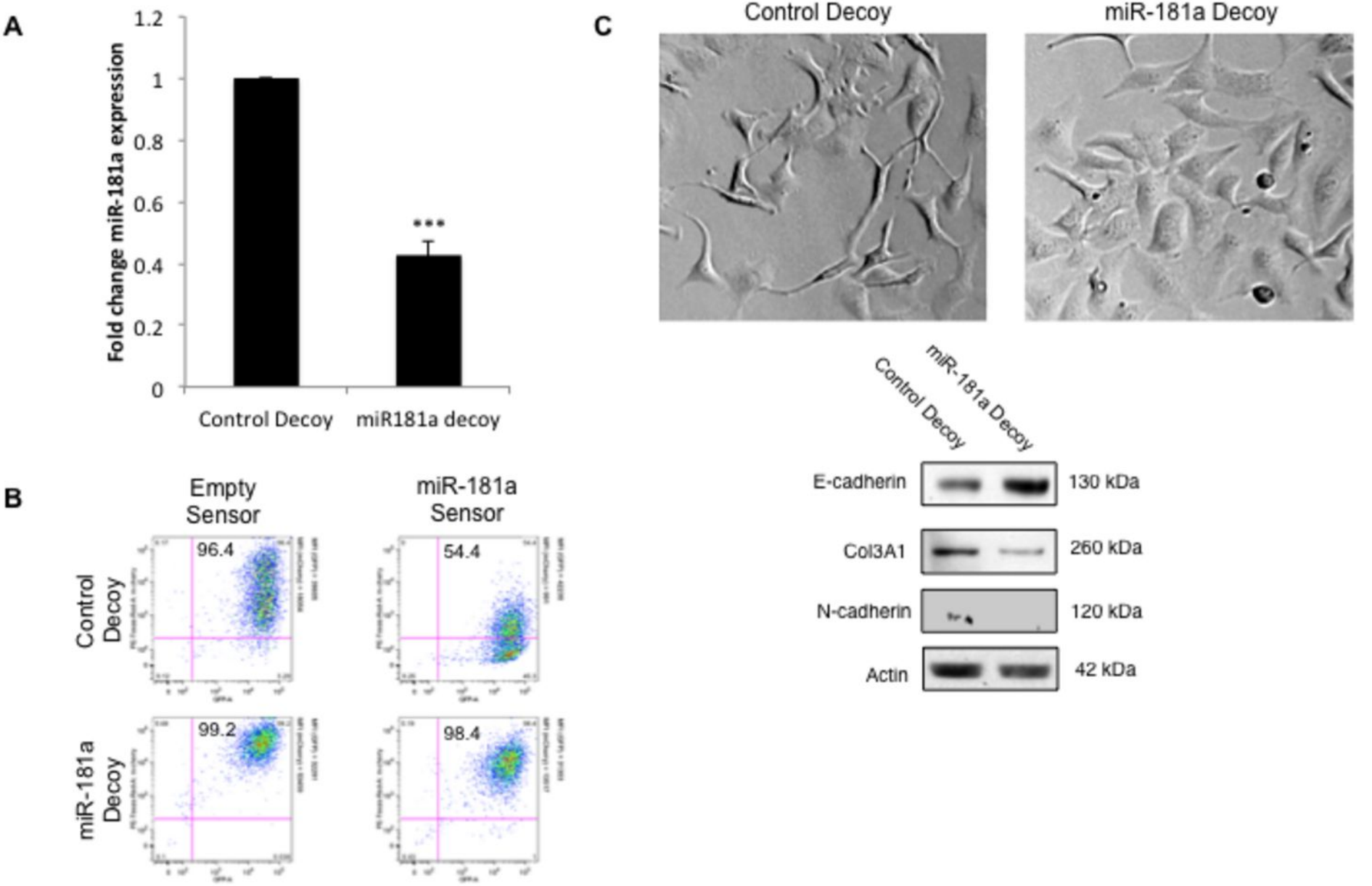
A
Fold change miR-181a expression
1.2
1
0.8
0.6
0.4
0.2
0
***
Control Decoy
miR181a decoy
B
Empty Sensor
miR-181a Sensor
Control Decoy
miR-181a Decoy
96.4
54.4
99.2
98.4
C
Control Decoy
miR-181a Decoy
E-cadherin
130 kDa
Col3A1
260 kDa
N-cadherin
120 kDa
Actin
42 kDa

Figure 2

D

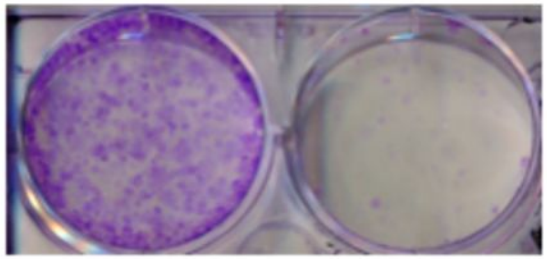
Control Decoy
miR-181a Decoy

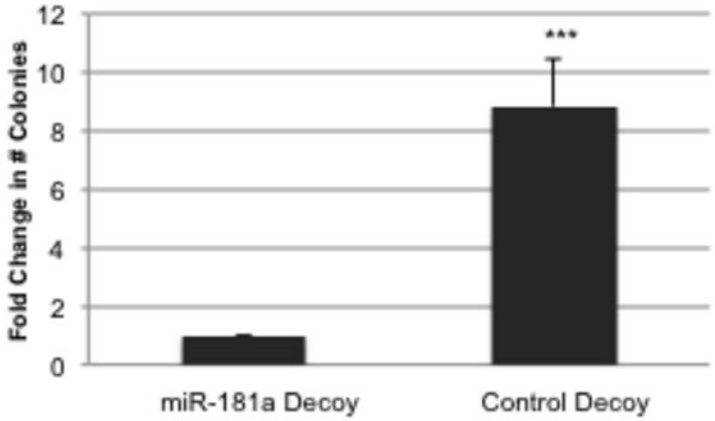
Fold Change in # Colonies
12
10
8
6
4
2
0
***
miR-181a Decoy
Control Decoy

E

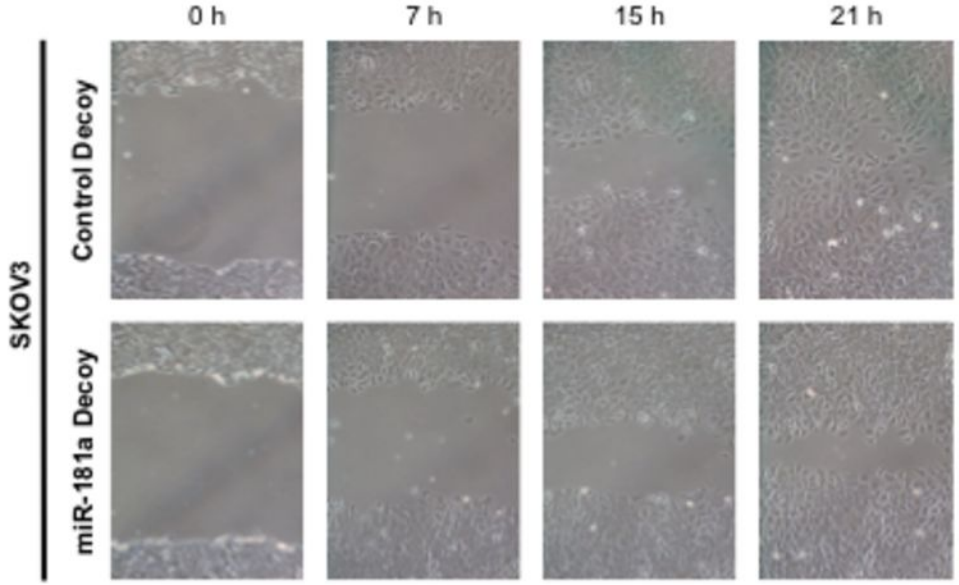
0 h
7 h
15 h
21 h
SKOV3
Control Decoy
miR-181a Decoy

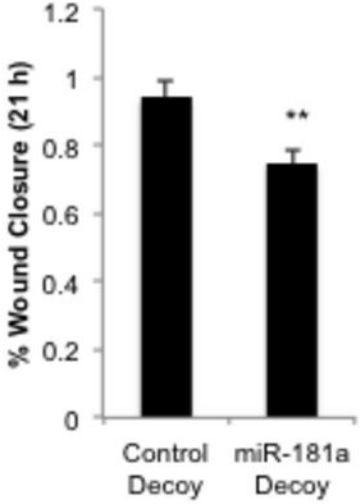
% Wound Closure (21 h)
1.2
1
0.8
0.6
0.4
0.2
0
**
Control Decoy
miR-181a Decoy

Figure 3

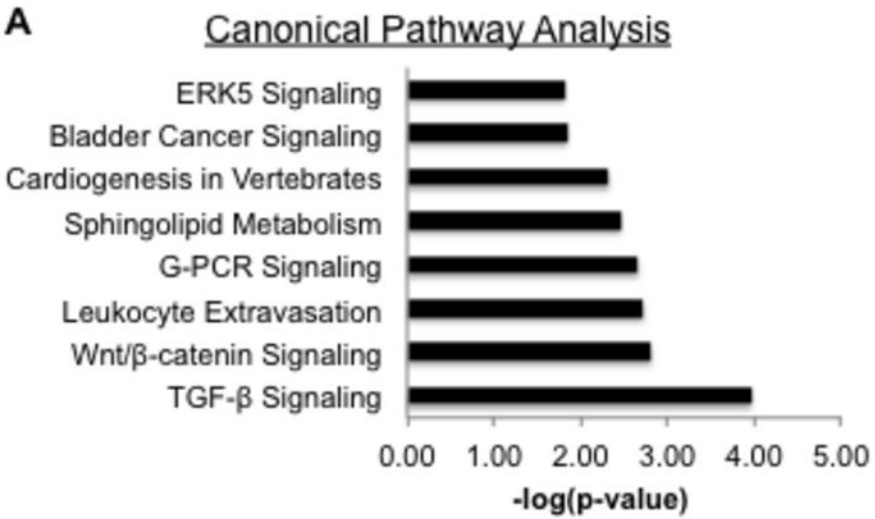
A
Canonical Pathway Analysis
ERK5 Signaling
Bladder Cancer Signaling
Cardiogenesis in Vertebrates
Sphingolipid Metabolism
G-PCR Signaling
Leukocyte Extravasation
Wnt/β-catenin Signaling
TGF-β Signaling
0.00 1.00 2.00 3.00 4.00 5.00
-log(p-value)

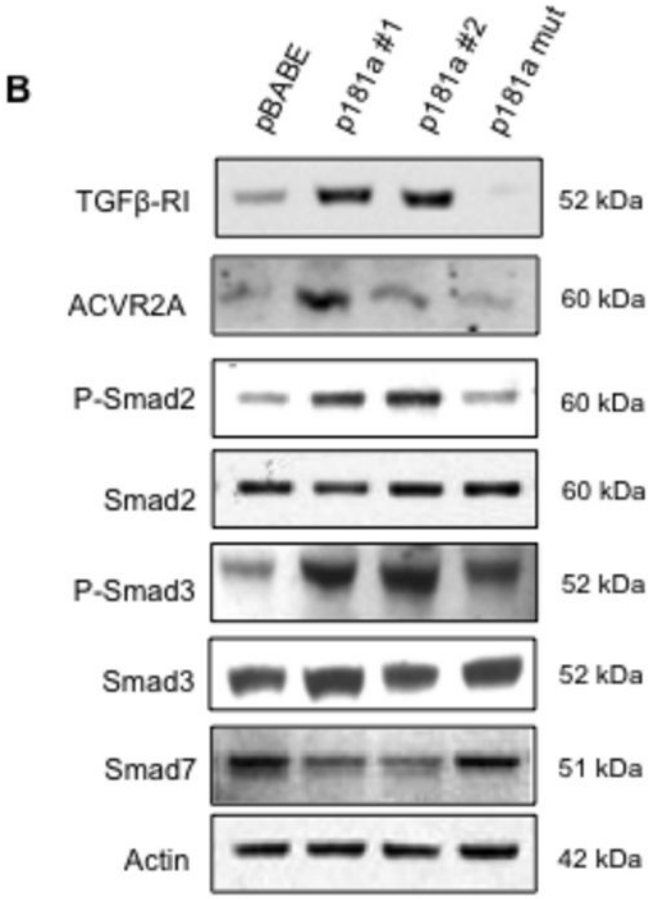
B
pBABE
p181a #1
p181a #2
p181a mut
TGFβ-RI
52 kDa
ACVR2A
60 kDa
P-Smad2
60 kDa
Smad2
60 kDa
P-Smad3
52 kDa
Smad3
52 kDa
Smad7
51 kDa
Actin
42 kDa

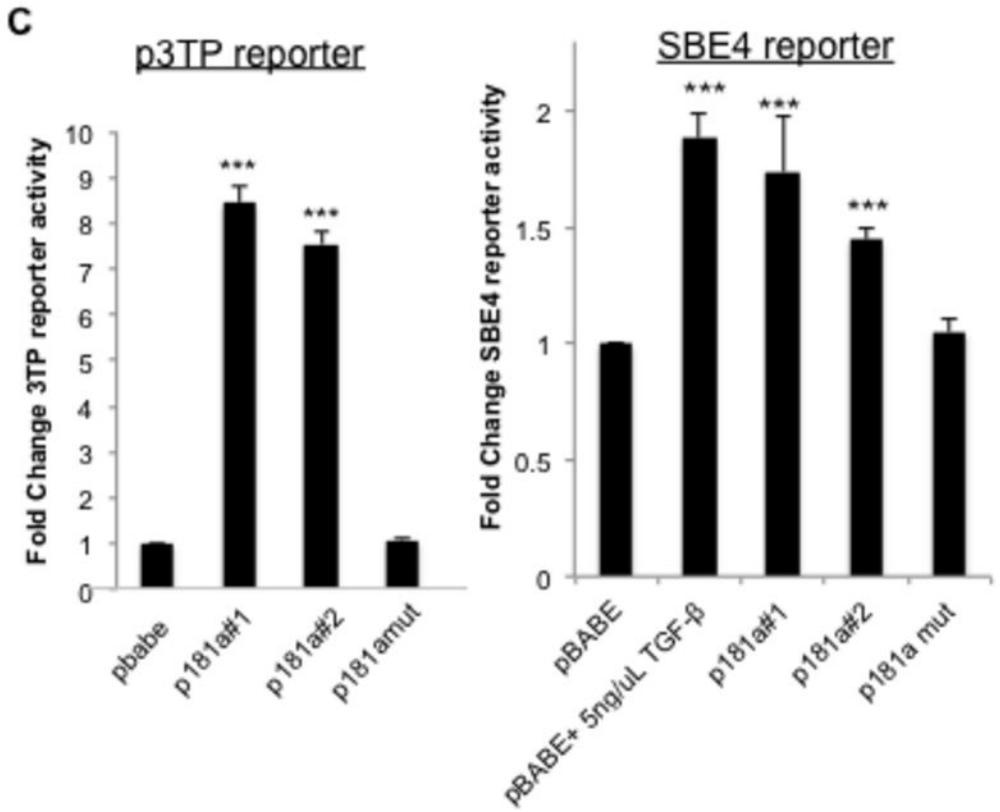
C
p3TP reporter
Fold Change 3TP reporter activity
***
***
pbabe
p181a#1
p181a#2
p181amut
SBE4 reporter
Fold Change SBE4 reporter activity
***
***
***
pBABE
pBABE+ 5ng/uL TGF-β
p181a#1
p181a#2
p181a mut

Figure 3

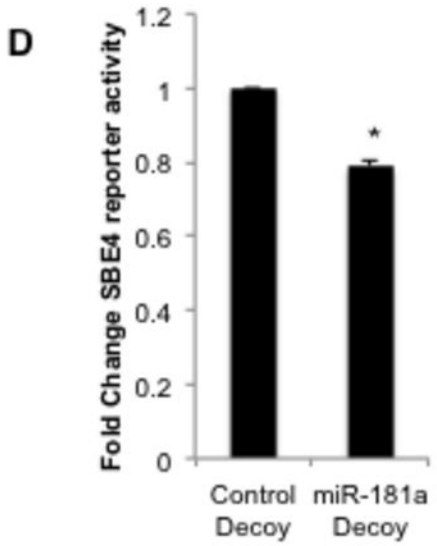
D
Fold Change SBE4 reporter activity
1.2
1
0.8
0.6
0.4
0.2
0
*
Control Decoy
miR-181a Decoy

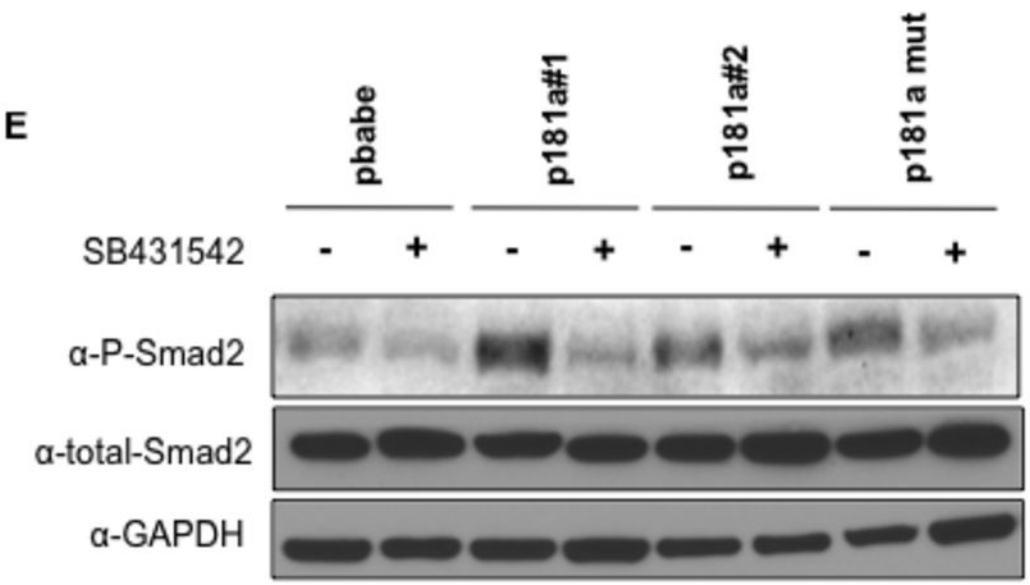
E
pbabe
p181a#1
p181a#2
p181a mut
SB431542
- + - + - + - +
α-P-Smad2
α-total-Smad2
α-GAPDH

Figure 3

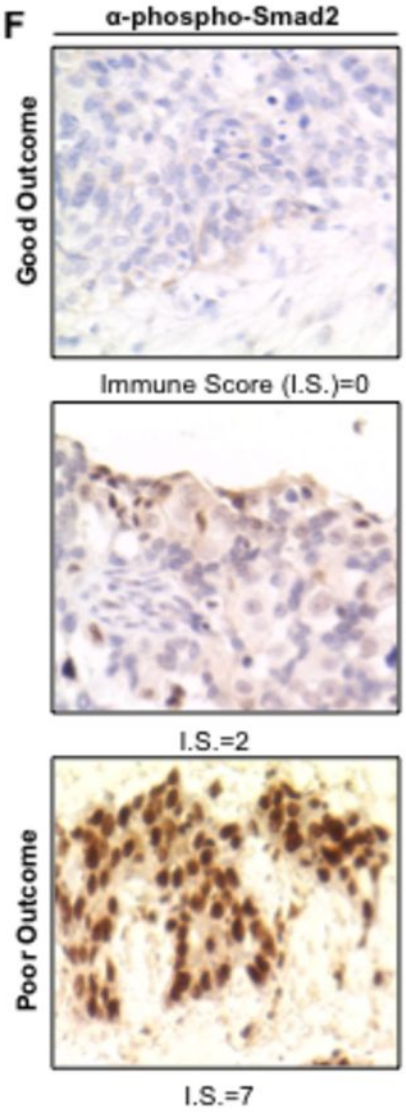

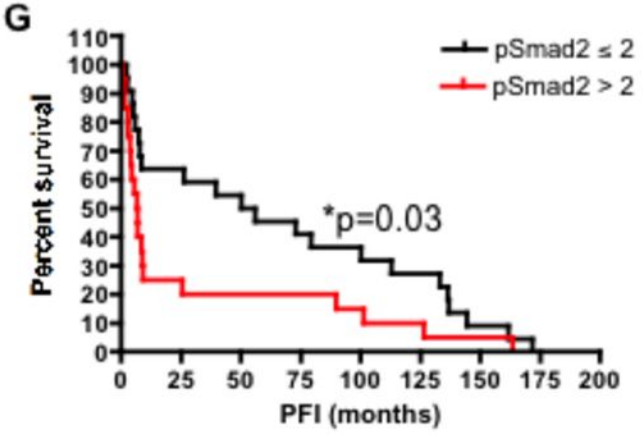

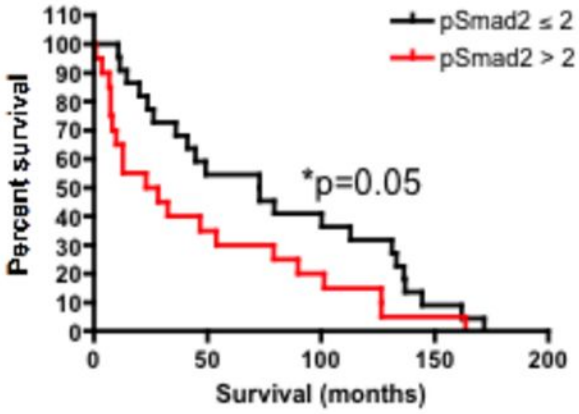

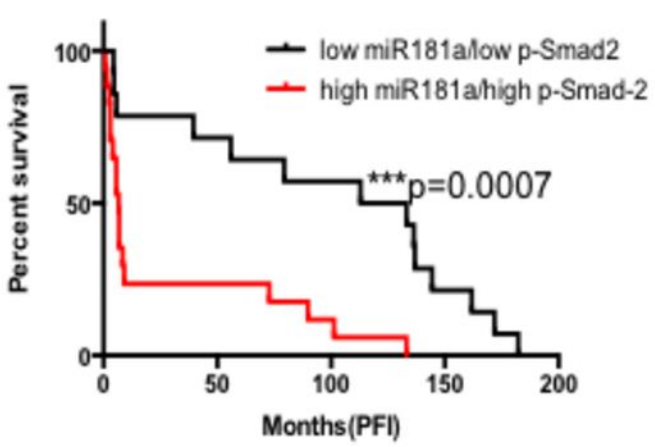

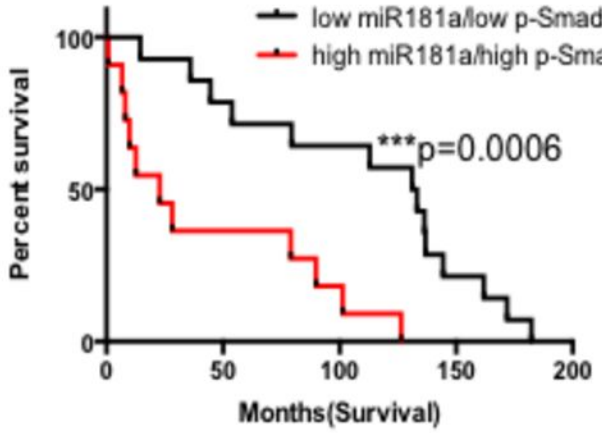

	P-Smad2 (I.S. < 2)	P-Smad2 (I.S. ≥ 2)
Median PFS	53.1	6.7
*P=0.03, OR 7.9; 95% CI: 7.4 to 8.5		
Median Survival	72.8	25.5
*P=0.05, OR 2.9; 95% CI: 2.3 to 3.4		

	low miR-181a/ low P-Smad2	high miR-181a/ high P-Smad2
Median PFS	123.1	6.6
***P=0.0007, OR 18.7; 95% CI: 9.2 to 37.8		
Median Survival	132.2	22.8
***P=0.0006, OR 5.8; 95% CI: 2.6 to 12.8		

Figure 4

A

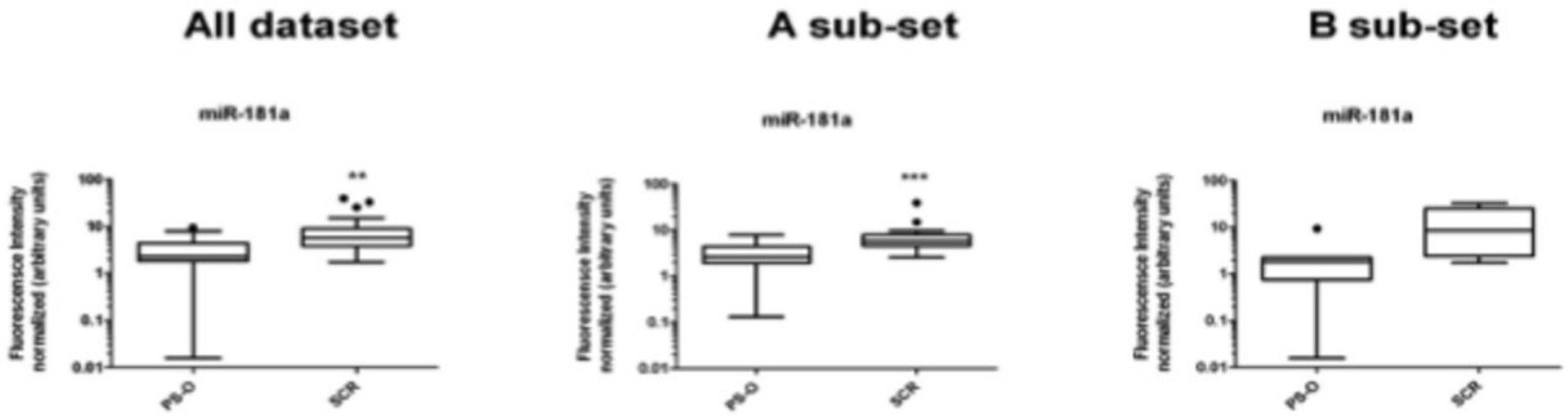

B

Gene name	Status	All dataset (n = 23)			A Group (EMT enriched; n=16)			B Group (n=7)		
		Median (IQ-range)	R	*p*	Median (IQ-range)	R	*p*	Median (IQ-range)	R	*p*
miR-181a	PS-O	2.263 (1.831-4.425)	2.51	0.0024	2.626 (1.919-4.464)	2.16	0.0006	1.831 (0.750-2.263)	4.74	0.063
	SCR	5.685 (3.774-8.904)			5.682 (4.492-7.953)			8.695 (2.410-25.34)		

Figure 5

A

Predicted miR-181a target genes in the TGF-β pathway

Gene ID	Symbol	Fold Change	sPCC*
NM_005904	SMAD7	-30.9	-6.2
NM_001106	ACVR2B	-8.9	14.8
NM_001616	ACVR2A	-7.1	-4.9
NM_001204	BMPR2	-2.6	-7.9
NM_001130916	TGFBR1	+2.1	-2.5

•Summed Pearson Correlation Coefficient determined by miRConnect analysis (miRConnect.org)

B

Smad7 3'UTR 5'…GUGUUAUCACCUAGC**UGAAUGU**U…3'

miR-181a 3' UGAGUGGCUGUCGCA**ACUUACA**A 5'

Mutant miR-181a 3' UGAGUGGCUGUCGCA**ACUUAAGG** 5'

Conservation

hsa 5'…GUGUUAUCACCUAGC**UGAAUGU**U…3'
mmu 5'…GUGUUAUCACCUAGC**UGAAUGU**U…3'
rno 5'…GUGUUAUCACCUAGC**UGAAUGU**U…3'
ptr 5'…GUGUUAUCACCUAGC**UGAAUGU**U…3'
mml 5'…GUGUUAUCACCUAGC**UGAAUGU**U…3'
Oan 5'…GUGUUAUCACCUAGC**UGAAUGU**U…3'

C

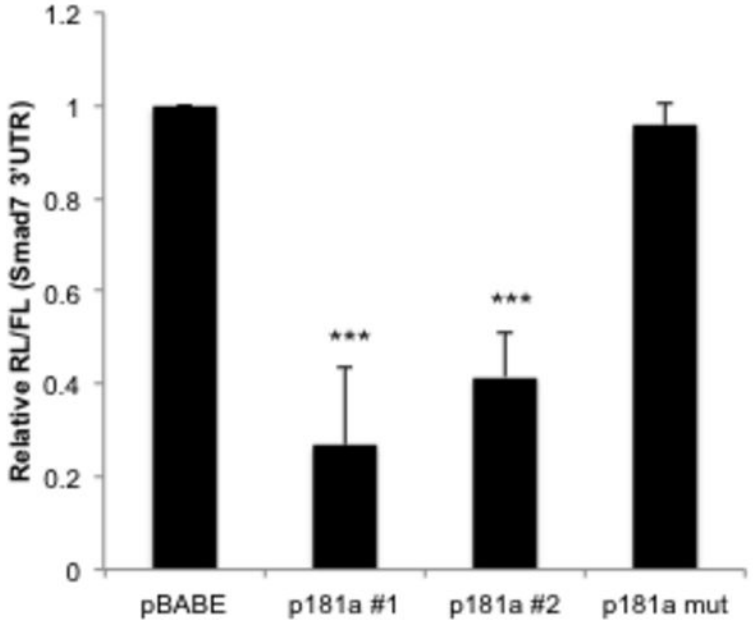

D

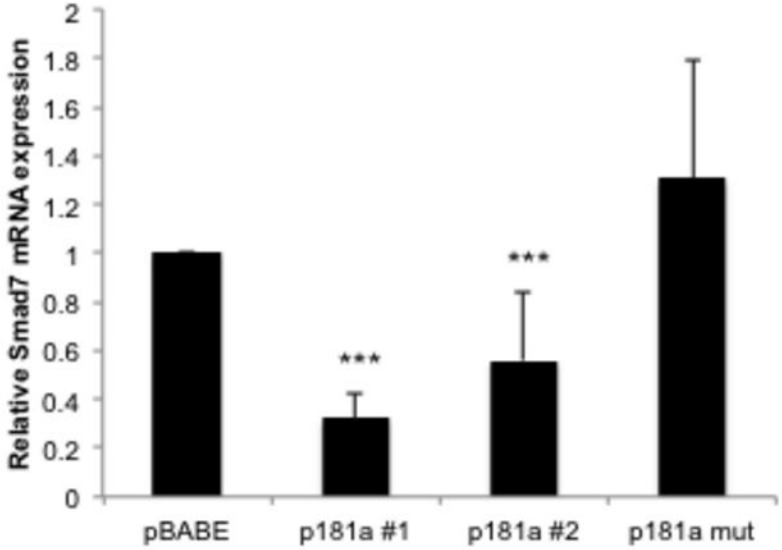

Figure 5

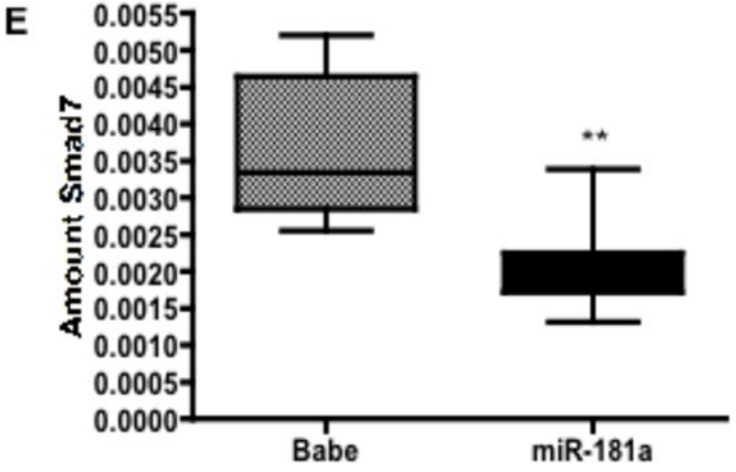
E
Amount Smad7
0.0055
0.0050
0.0045
0.0040
0.0035
0.0030
0.0025
0.0020
0.0015
0.0010
0.0005
0.0000
**
Babe
miR-181a

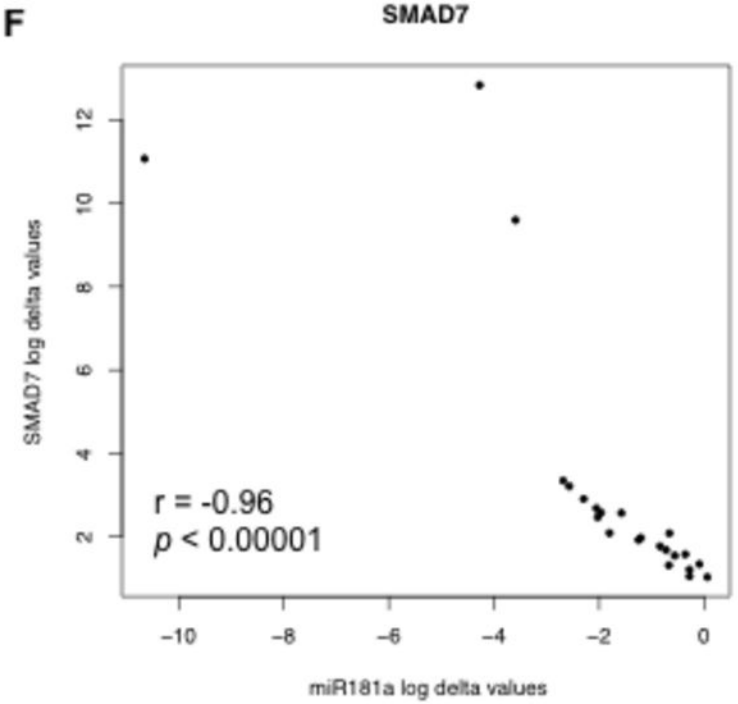
F
SMAD7
SMAD7 log delta values
12
10
8
6
4
2
r = -0.96
p < 0.00001
−10
−8
−6
−4
−2
0
miR181a log delta values

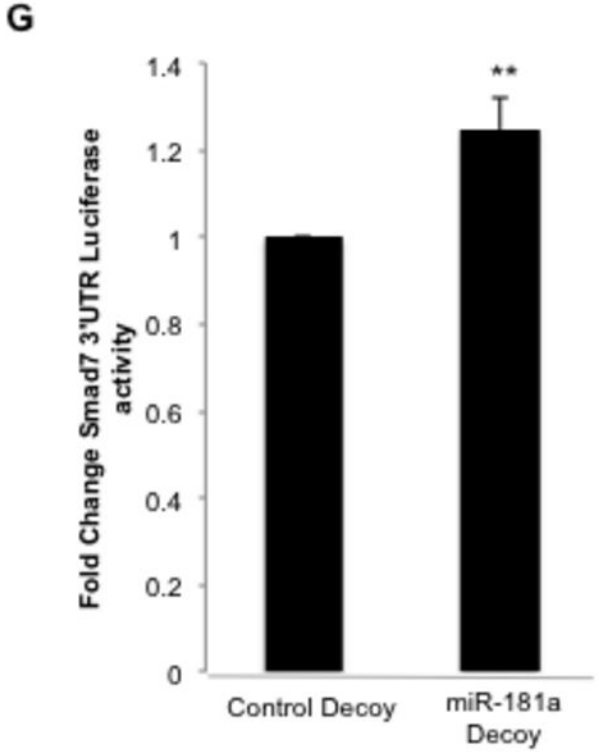
G
Fold Change Smad7 3'UTR Luciferase activity
1.4
1.2
1
0.8
0.6
0.4
0.2
0
**
Control Decoy
miR-181a Decoy

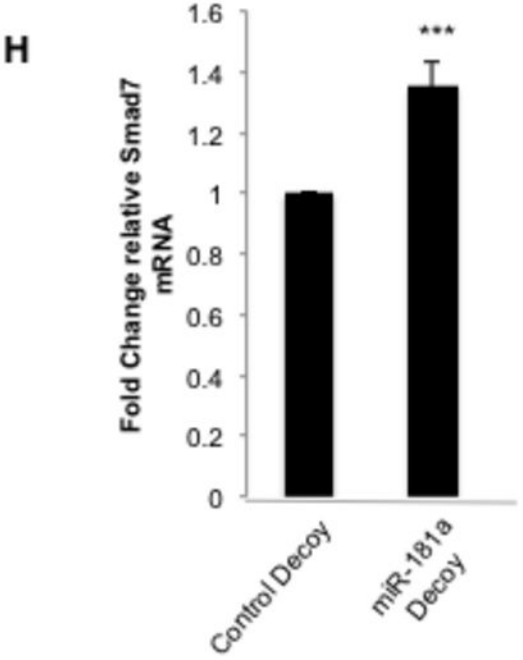
H
Fold Change relative Smad7 mRNA
1.6
1.4
1.2
1
0.8
0.6
0.4
0.2
0
***
Control Decoy
miR-181a Decoy

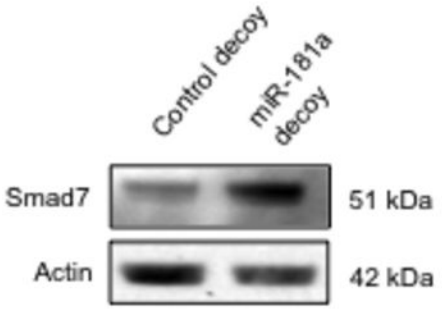
Control decoy
miR-181a decoy
Smad7
51 kDa
Actin
42 kDa

Figure 6

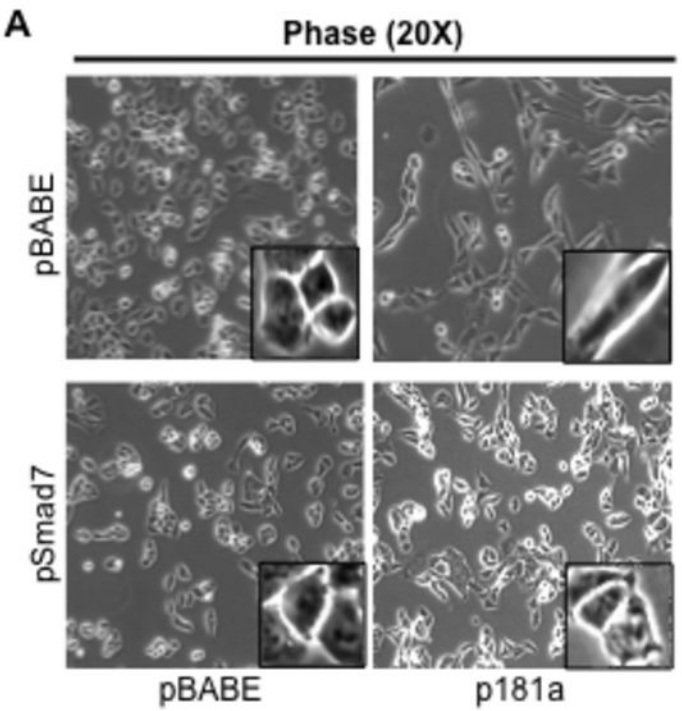
A
Phase (20X)
pBABE
pSmad7
pBABE
p181a

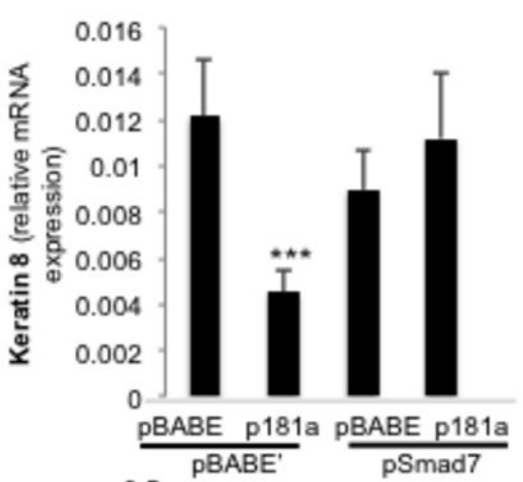
Keratin 8 (relative mRNA expression)
0.016
0.014
0.012
0.01
0.008
0.006
0.004
0.002
0
***
pBABE p181a pBABE p181a
pBABE'
pSmad7

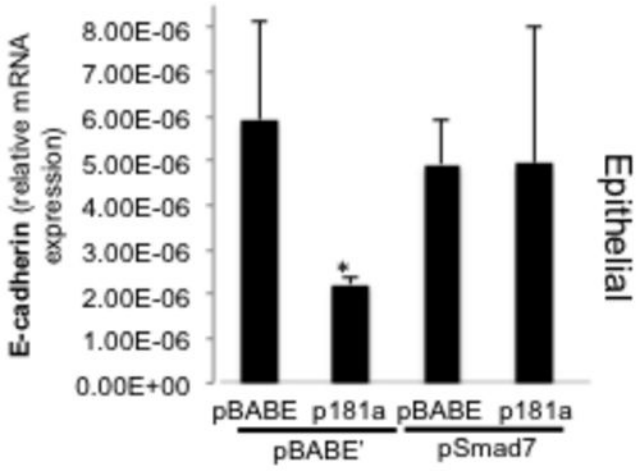
E-cadherin (relative mRNA expression)
8.00E-06
7.00E-06
6.00E-06
5.00E-06
4.00E-06
3.00E-06
2.00E-06
1.00E-06
0.00E+00
*
pBABE p181a pBABE p181a
pBABE'
pSmad7
Epithelial

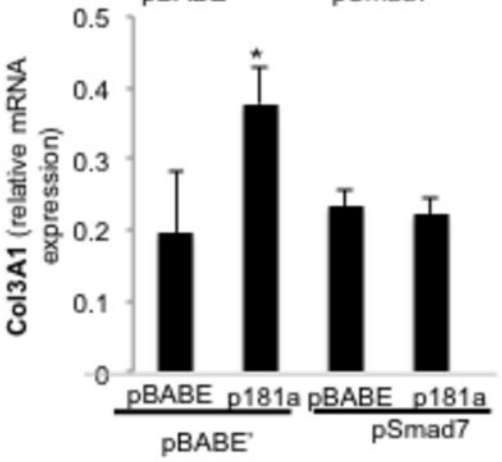
Col3A1 (relative mRNA expression)
0.5
0.4
0.3
0.2
0.1
0
*
pBABE p181a pBABE p181a
pBABE'
pSmad7

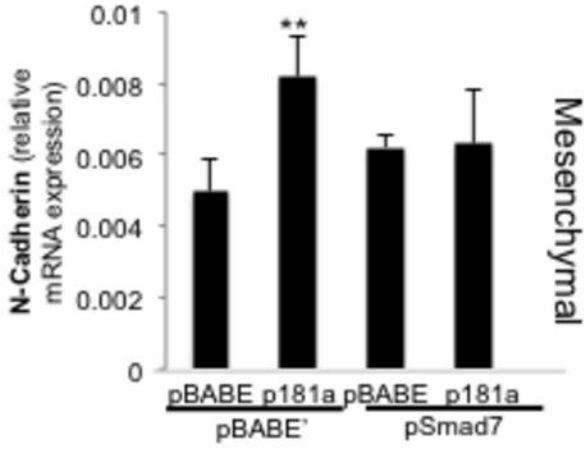
N-Cadherin (relative mRNA expression)
0.01
0.008
0.006
0.004
0.002
0
**
pBABE p181a pBABE p181a
pBABE'
pSmad7
Mesenchymal

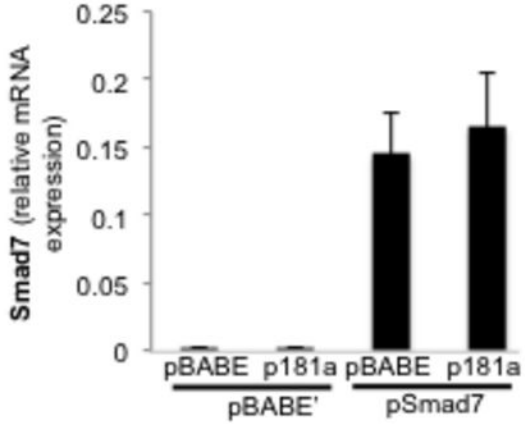
Smad7 (relative mRNA expression)
0.25
0.2
0.15
0.1
0.05
0
pBABE p181a pBABE p181a
pBABE'
pSmad7

Figure 6

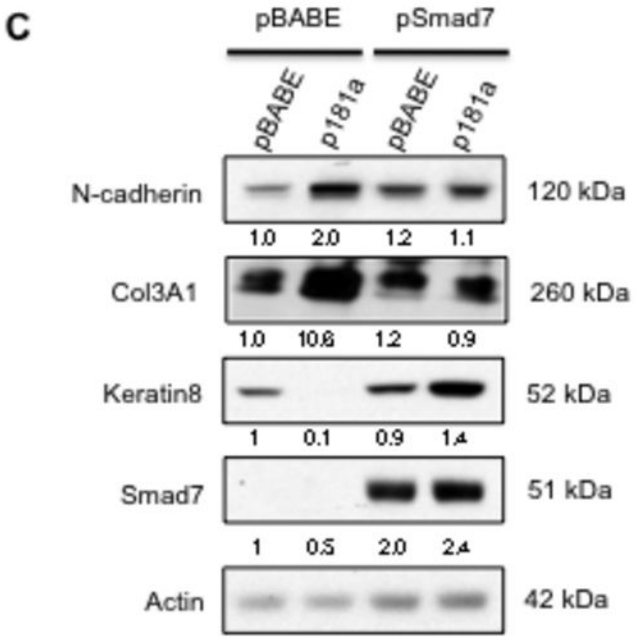
C
pBABE
pSmad7
pBABE
p181a
pBABE
p181a
N-cadherin
120 kDa
1.0 2.0 1.2 1.1
Col3A1
260 kDa
1.0 10.8 1.2 0.9
Keratin8
52 kDa
1 0.1 0.9 1.4
Smad7
51 kDa
1 0.5 2.0 2.4
Actin
42 kDa

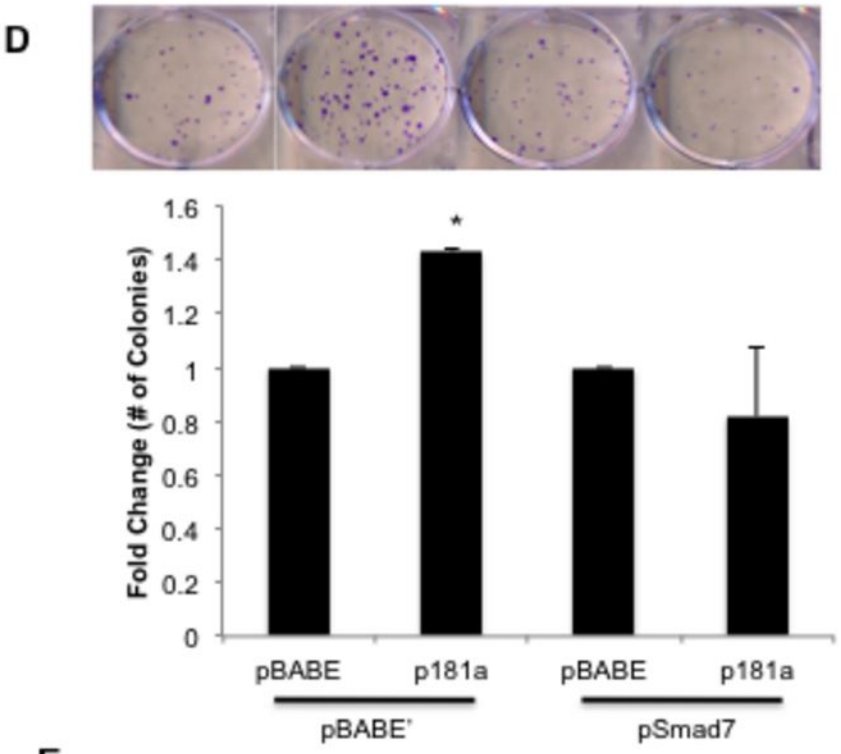
D
Fold Change (# of Colonies)
1.6
1.4
1.2
1
0.8
0.6
0.4
0.2
0
*
pBABE
p181a
pBABE
p181a
pBABE'
pSmad7

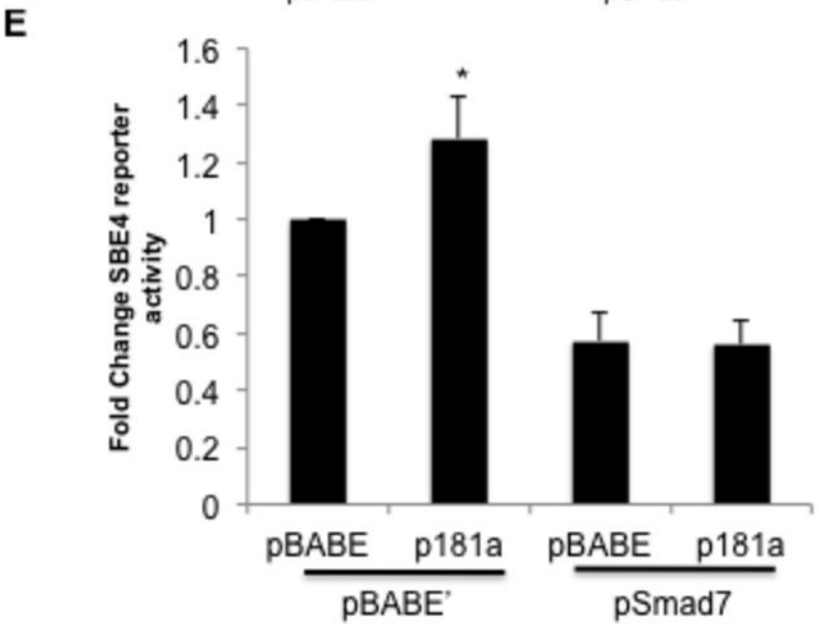
E
Fold Change SBE4 reporter activity
1.6
1.4
1.2
1
0.8
0.6
0.4
0.2
0
*
pBABE
p181a
pBABE
p181a
pBABE'
pSmad7

A Reflectance Based Method for Label Free Detection of Low Abundance MicroRNA Biomarkers

Robert Purnell[1]*, Christine Lee[2], Julian D. Down[1], Naresh Menon[1] and Analisa DiFeo[2]

[1]ChromoLogic LLC, 180 N. Vinedo Ave., Pasadena, CA 91107

[2]Case Comprehensive Cancer Center, 2103 Cornell Road Cleveland, Ohio 44106

A magnetic bead-based nucleic acid screening with Amplified Reflectometric Interference Analysis (ARIA) for quantification of multiple microRNA biomarkers at unprecedented sensitivity and specificity is described. The ARIA subsystem is an optically pumped ring fiber laser coupled to a sensor that measures the concentration of microRNA as a change in the resonance frequency of the optical cavity. This enabled detection of microRNA levels in biological samples at subfemtomolar concentrations and surpassed the sensitivity of the standard Taqman/RT-PCR assay.

Keywords

Amplified Reflectometric Interference Analysis, circulating microRNA, ovarian cancer

MicroRNAs (miRNAs) are non-coding RNAs of 18-22 nucleotides that regulate diverse cellular processes including development, proliferation and differentiation [1]. They have been detected in a range of body fluids such as blood plasma/sera and have been successfully used as biomarkers for various physiological conditions, including pregnancy [2], diabetes [3], radiation sickness [4], and numerous forms of cancer [5]. In cancer, circulating miRNAs will undoubtedly play a significant role in clinical applications such as disease diagnostics, monitoring therapeutic

effect and predicting recurrence in cancer patients. Numerous studies have established correlation between abnormal levels of circulating miRNAs in the blood and the type of cancer, its stage of development, and chemoresistance [5-11]. In addition, miRNA expression profiles are altered at the earliest stages of cancer development, providing an opportunity to meet the challenges imposed by difficult to diagnose malignancies such as ovarian and pancreatic tumors [5-11]. Circulating miRNAs in blood plasma are easily obtainable for analysis and are additionally protected in exosomes, microparticles, and nucleoprotein complexes [12], conferring high stability at room temperature for days and even after several freeze-thaw cycles [6]. These qualities make circulating miRNAs attractive biomarkers for early diagnosis and monitoring of cancer patients, which could dramatically improve the quality of treatment and reduce mortality rate. Unfortunately, the current methods used for evaluation of miRNA in body fluids such as RT-PCR are labor intensive and have limited accuracy, mostly attributed to the requirement for extensive pre-amplification cycles.

Recent research has focused on development of electrically and optically-based "direct detection" methods, including Arrayed Surface Plasmon Resonance Imaging (SPRI)[13][14], Nanoparticle-Enhanced SPR [15], Nanoporous silicon [16], and Nanowires [17][18]. In these schemes, targeted biomarkers present in low abundance are detected in a heterogenous sample through binding to biochemical probes (e.g., cDNA, peptide nucleic acid (PNA), proteins) chemically linked to a nanofabricated and biochemically active sensor substrate. Changes in the optical or electrical characteristics of the sensor following binding of the biomarker and probe are then used to quantify its concentration. These technologies have successfully demonstrated attomolar (10^{-18}) [15] to femtomolar (10^{-15}) [18] sensitivity without the use of expensive and time intensive preparation and enzymatic reaction steps. Importantly, eliminating the enzyme also

increases versatility of the assay, enabling implementation in microfluidic, lab-on-a-chip devices for Point-of-Care diagnostics and high throughput screening applications; an example is Flow-Injection SPR [19].

In spite of significant progress in this area, many of these platforms suffer several critical limitations in sensitivity, user friendliness, and cost that preclude widespread implementation in clinical diagnostics. To address these limitations and fully utilize the diagnostic potential of miRNA biomarkers, we have developed and patented [20][21] a novel, label-free technique based on Amplified Reflectometric Interference Analysis (ARIA). In the ARIA system, a narrow line-width Erbium-doped single mode fiber ring laser [22] is coupled to a removable borosilicate glass based substrate with a fiber-coupled micro-optic lens assembly. This substrate, henceforth known as the 'ARIA sensor', is coated with ceramic layers with nanometer level precision in order to make it a Bragg (partial) reflector. The ARIA sensor forms an integral part of the lasing cavity and, based on the light coupled back into the resonating ring by reflection, determines the lasing frequency of the fiber ring laser. The reflection properties of the ARIA sensor is designed to be extremely sensitive to the refractive index (RI) and optical density of any analyte placed on the surface of the ARIA sensor [22]. Since concentrations of free RNA and DNA correlate with refractive index and optical density of a sample [23], changes in the concentration of RNA/DNA biomarkers result in a predictable change in the wavelength of the reflected signal and a corresponding change in the lasing frequency of the fiber ring laser.

In this study, we introduce the ARIA concept, verify subfemtomolar detection limits using synthetic ssDNA standard solutions, and test the system on miRNA biomarkers correlated with 1) cisplatinum resistance in human ovarian cancer cell lines and 2) ovarian tumor burden in an *in vivo* human tumor xenograft mouse model.

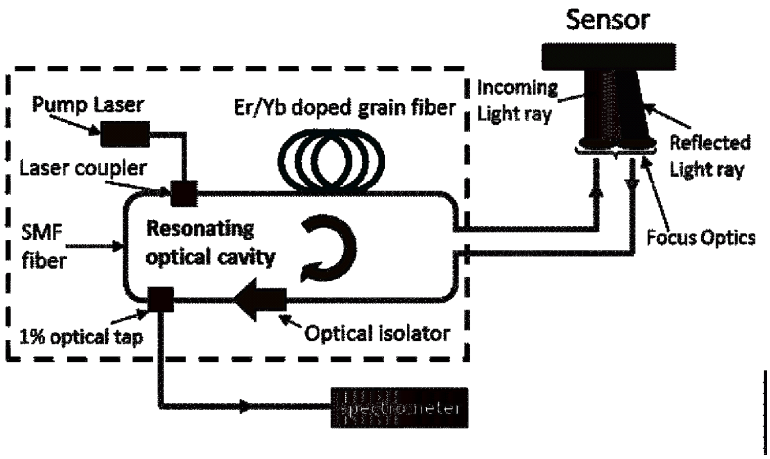

Figure 1. Diagram of CL's patented ARIA detection platform. The ARIA is comprised of Erbium-doped and single mode optical fiber arranged in a ring fiber laser configuration with optical components. The ring fiber laser is optically pumped using a 980 nm laser diode, which generates a lasing cavity with a resonant wavelength between 1500 and 1600nm (see text). The ring fiber laser is optically coupled to a glass substrate (ARIA sensor, see Figure 2) so that changes in the concentrations of biomarker induce changes in the resonance frequency of the laser.

At its core, the ARIA system (Figure 1) is a ring fiber laser assembled from a 20m Erbium-doped optical fiber (IsoGain4, Fibercore, Half Moon Bay, CA) and single mode fiber (SMF-28, Fibercore, Halfmoon Bay, CA) arranged in a close-loop configuration. A 980nm diode laser (Model PL980P330J, Thorlabs, New Jersey) is fiberoptically coupled to the ring, which optically pumps the Erbium gain fiber causing it to produce stimulated emission at its characteristic wavelength (1500nm – 1600nm) [22]. Light from the fiber-ring is coupled to the ARIA sensor (discussed further below) using a Gradient Index (GRIN) lens (Edmund Optics, New Jersey). The wavelength of the light reflected back from the sensing surface is modulated by the

refractive index (RI) and optical density of the analyte placed on the surface because of reflectometric interference [23]. Since concentration of free RNA and DNA correlate with the RI [24] and optical density of the solution, changes in the concentration of biomarkers result in a predictable change in the peak wavelength of the reflected signal. Reflectometric interference is a well-understood phenomenon and is partially responsible for the bright bands of colors seen on water when a small drop of oil (thin-film) is placed on it. When the reflected light from the sensing surface is coupled back into the closed loop ring it is further amplified by the optically pumped Erbium gain fiber, forming a closed loop resonating cavity. The double pass gain of this closed loop cavity is related to the single pass gain (G), wavelength reflectance (R), cavity length (L) and passive loss (alpha) as shown in equation 1:

$$gain(\lambda) \approx G(\lambda)^2 \mathrm{Re}^{(-2\alpha(\lambda)L)} \qquad \text{(Equation 1)}$$

From Equation 1, we note that a closed-loop cavity begins to resonate and lase at a wavelength (λ) that corresponds to the wavelength at which the cavity has the lowest loss. The excited emissions are reflected back by the ARIA sensing surface travel clock-wise along the single mode fiber (SMF) in a direction set by the optical isolator (Figure 1). This causes the fiber-ring to resonate at a wavelength reflected back from the base of the ARIA sensor, thereby amplifying the peak signal at the lasing wavelength. To measure this wavelength, the fiber ring laser is monitored using an optical 1% tap connected to an optical spectrum analyzer (Anritsu MS9710B). While similar in concept/principle to the biocavity laser [20] developed by Gourley et. al., in the ARIA system, the measurement region is placed *outside* the lasing cavity while still perturbing the cavity by the extension of the evanescent field at the reflectors into the analyte (interaction region).

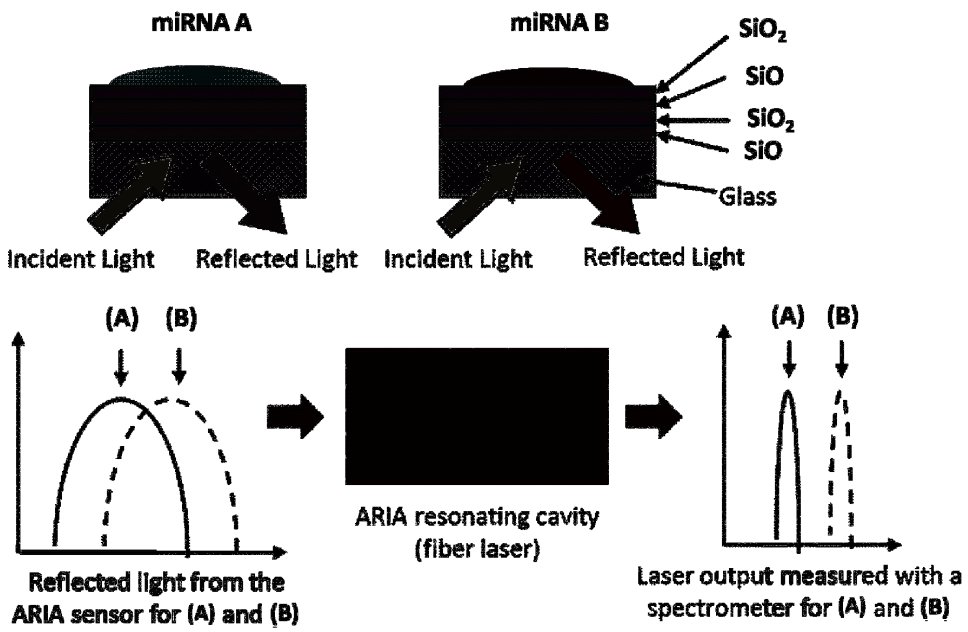

Figure 2. Conceptual Diagram of ARIA Concept. The base of the ARIA sensor is comprised of a planar glass with alternating layers of SiO and SiO_2 deposited by cold-plasma sputtering. Changes in concentration of miRNA biomarkers in the sample cause a response in the peak of the raised-cosine Bragg reflected spectra local to each well. When combined with the fiber laser resonating cavity (see Figure 1), this broad reflection results in a high signal to noise ratio (SNR) laser peak output change that can be used easily for quantifying distinct miRNA samples A and B.

To adapt the ARIA system for measurement of miRNA biomarkers, ARIA sensors were fabricated by depositing alternating layers of layers of SiO_2 and SiO (see Figure 2) onto a borosilicate glass microscrope slide by cold plasma sputtering (Schott North America Inc., Elmsford NY). This converts the glass slide into a partial Bragg reflector. The thicknesses of the alternating layers are designed specifically to generate a wavelength dependent reflectance response in the 1500-1600nm Er:Yb operating regime (reflectometric interference [18]), which is

highly sensitive to changes in the optical density and RI at the surface. The Bragg wavelength is given by Equation 2:

$$\lambda_B \propto 2\Lambda A(n,c) \qquad \text{Equation. 2}$$

where Λ is the period of the perturbation determined by the ceramic thin-film coating and A is the optical length of the assay region that is a function of the refractive index (n) and optical density (c) of an assay. Figure 2 shows a performance schematic of the Bragg reflector integrated with the ARIA sensor. The combination of the lasing material and the reflector design on the ARIA sensor enables the correlation of the lasing frequency to the concentrations of miRNA biomarker A and B. The cost of the reflecting surface is of the order of a microscopic slide making it extremely appealing for use as a disposable component in any miRNA diagnostic kit. As a result, the ARIA sensor and ring fiber laser form a low-cost, highly sensitive detector.

ARIA calibration testing on ssDNA standards

To demonstrate the sensitivity of the ARIA system for detection of miRNA at physiological concentrations (< 1 fM), we investigated the response of the ARIA system to solutions of 30-base ssDNA oligomers (Integrated DNA Technologies, Coralville, IA) designed to mimic miRNA (sequence (5') ACATCGTTACCAGACAGTGTTA-(3')). ssDNA solutions were diluted in deionized water at concentrations of 100 fM, 10 fM, 5 fM, and 0.01 fM - typical concentrations of circulating miRNA cancer biomarkers [5] [21]. The ARIA response is highly sensitive to the position of the sensor and micron scale non-uniformities in the sensor, as minute changes to the properties of the lasing cavity (e.g., lasing cavity length (see Equation 1)) can generate shifts in the peak wavelength. To compensate for these variations, we performed background calibration measurements at each sample position by recording 50 spectra at each sampling position before addition of ssDNA samples (see Figure 3A). After calibration

measurements were complete, we deposited 1.3µL volumes of the ssDNA calibration standards and DI water solutions in triplicate on the ARIA sensor as shown in Figure 3B. To prevent evaporation over the course of the scan, measurements were taken in a humidity controlled chamber positioned on top of the stage.

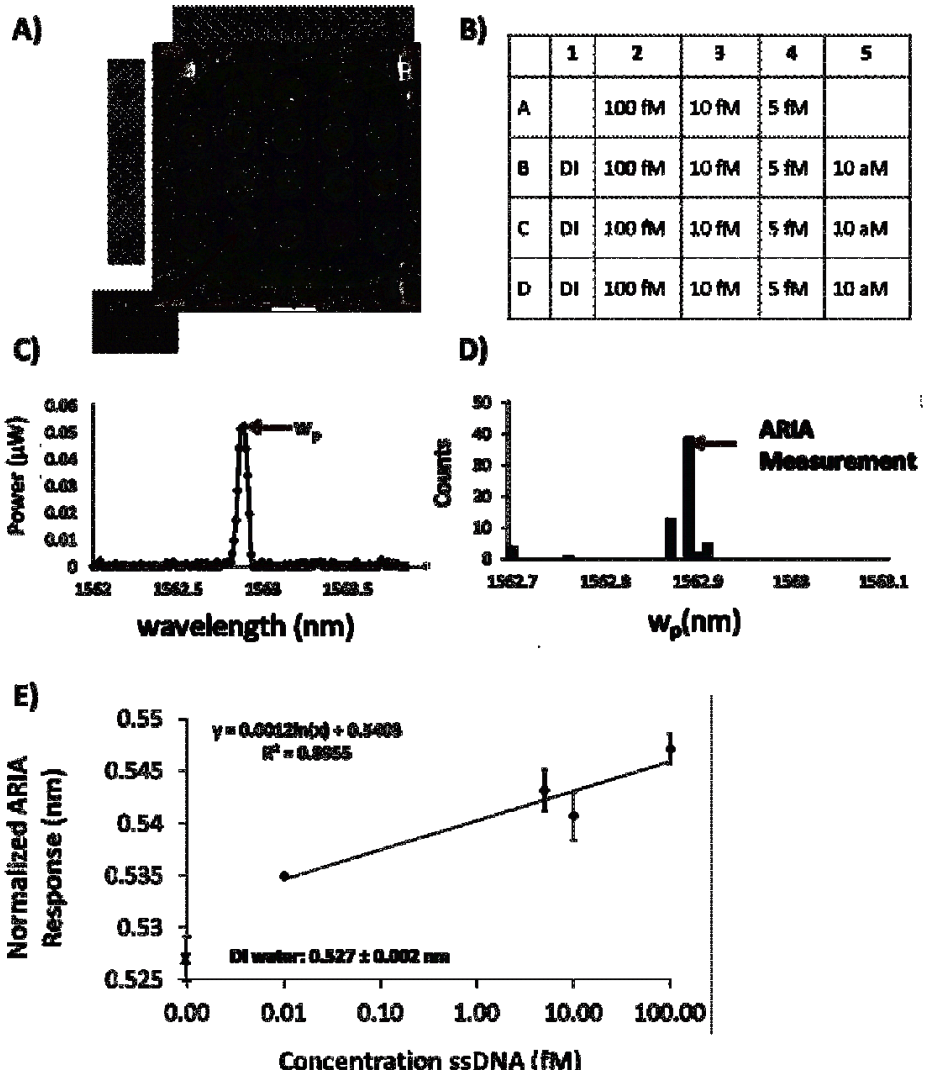

Figure 3. ARIA ssDNA calibration tests. A) 1.3µL samples are deposited on the ARIA sensor, with concentrations indicated in **(B)**. To extract the peak wavelength (w_p), a Gaussian fit is performed on each spectrum **(C)**. A histogram of all ARIA values **(D)** indicates an unambiguous value for w_p. **E)** A graph of average, background corrected Δw_p values (see text) for ssDNA

samples ranging in concentration from 10 to 100,000 aM, with DI water measurement included as a reference. Error bars were computed as the standard deviation of the 50 spectral measurements on three samples for each concentration.

To extract ARIA measurements from spectral data, we developed a Matlab-based program that algorithmically extracts the ARIA peak wavelength (w_p) by performing a Gaussian fit to each spectra and assigning the peak value as the ARIA response (Figure 3C). Background adjusted measurements (Δw_p) were computed by subtracting the average background measurements (w_{pb}) at each position from the average sample measurements (w_{ps}). Correction factors were also developed to compensate for other sources of variation in the signal, including mode hopping and drift due to changes in environmental conditions (see supplemental sections S1 and S2). ARIA measurements for the ssDNA calibration standards, as shown in the semi-log plot in Figure 3E, display a linear response with concentration (R^2 = 0.896) over 4 orders of magnitude of ssDNA concentration, with a minimum detection limit of 10 aM. An ARIA measurement of DI water is included on the graph for comparison. Importantly, unique measurements responses at 100 fM (Δw_p = 0.547 ± 0.001 nm) and 10 fM (Δw_p = 0.5407 ± 0.002 nm) indicate the ARIA system is capable of resolving femtomolar changes at concentrations of miRNA biomarkers in the blood circulation that typically range from 1000 to 100000 copies / μL [5][21].

miRNA capture using magnetic microbeads and validation in ovarian cancer cell lines.

Recent studies have uncovered miRNAs that are differentially expressed in chemotherapy resistant ovarian cancer cell lines, suggesting miRNA biomarkers could be used to monitor

chemotherapy response and therefore guide chemotherapy treatment and/or screen for tumor recurrence [8][9]. As shown in the survival curve in Figure 4A, CP70 cells display greater resistance to cisplatinum treatment as compared to the parental A2780 cell line (see supplemental section S3 for further details). A comparison of RNU6B-normalized RT-PCR measurements (n = 3) of miR-181a in growth media and cell lysate (see Figure 4B) indicate elevated expression levels of this miRNA are observed in both cell lysate and growth media. This suggests miR-181a is an ideal blood-based biomarker for cisplatinum resistance, and suitable for initial testing on the ARIA system. MiR-134, which is unrelated to cisplatinum sensitivity, (data not shown) will serve as an ovarian cancer specific positive control.

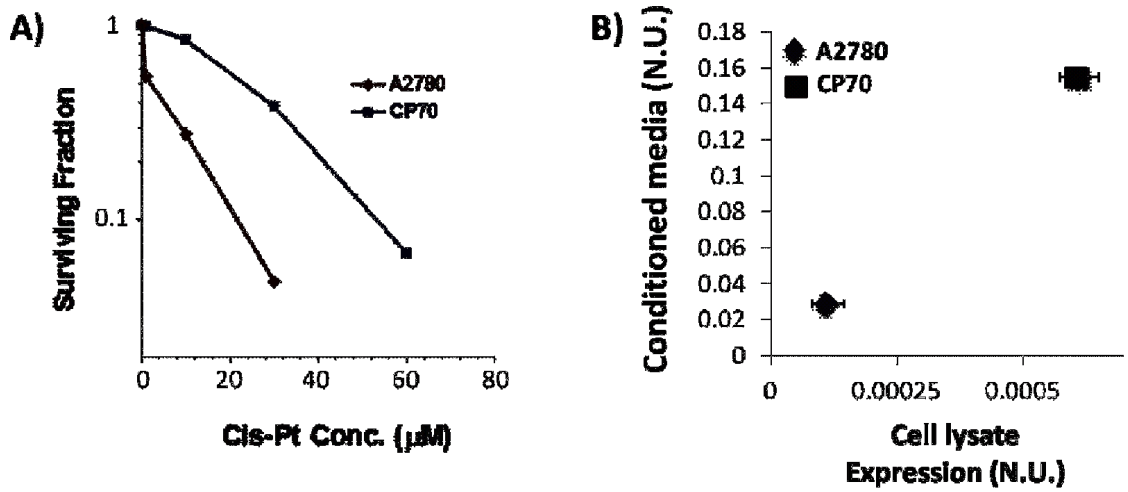

Figure 4. miR-181a expression in ovarian cancer cell lines. **(A)** Semi-log plot of the surviving fractions of A2780 and CP70 as demonstrated through the MTT assay (see supplemental S3 for further description), indicates enhanced cisplatinum resistance of the CP70 cell line, as observed previously [27]. **(B)** RT-PCR results for growth media and cell lysate are expressed as a fold difference (normalized units, N.U.) between miR-181a and RNU6B, which is invariant with cisplatinum resistance. Expression levels of miR-181a confirm an increase in this biomarker with cisplatinum resistance is observed in both cell lysate and growth media.

We developed a protocol based on magnetic microbead technology (Dynabeads, Invitrogen) to capture, concentrate and elute miRNA targets from a heterogeneous biological fluid samples (Figure 5) that can be directly dispensed onto an ARIA sensor with a pipette – thereby eliminating the need for any micro-arrayer or other cDNA spotting techniques. In this procedure, 2.8-μm diameter, streptavidin-coated magnetic microbeads are functionalized with cDNA probes specific to the miRNA target. To attach the cDNA probes, 500 μL of a 10 mg/mL microbead solution was mixed with 10 μL of a 10 μM solution of biotinylated cDNA probe complementary to the miRNAs targets (Integrated DNA Technologies, Coralville, IA) and dissolved in binding and wash buffer (BW buffer, composition: 2 M NaCl, 10 mM Tris, 1 mM EDTA, pH 7.0). This solution was then mixed gently on a shaker for 1 hr to ensure complete binding of microbeads with the cDNA. Binding efficiency of the beads was confirmed by magnetically separating the beads from solution using a neodymium magnet and measuring the change in the concentration of free cDNA in solution before and after binding using a Nanodrop benchtop spectrometer (Thermofisher, Inc). The measurements before (1489.6 ng/μL) and after (< 0.5 ng/μL, below background signal of the Nanodrop) this procedure indicate successful functionalization of the beads with cDNA.

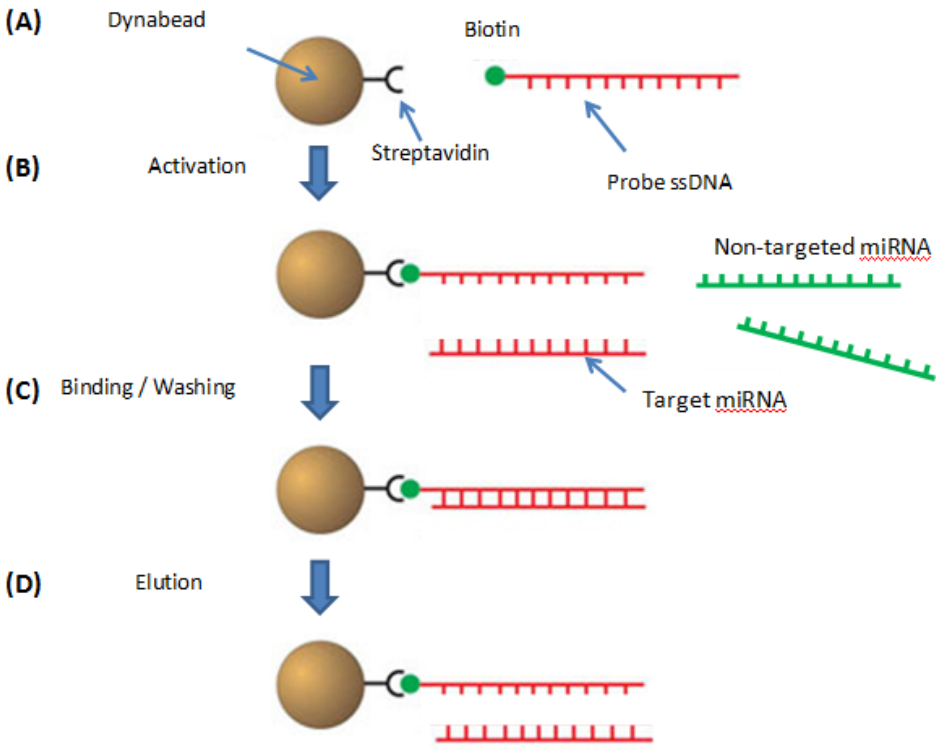

Figure 5. Extraction of miRNAs with magnetic microbeads. (A) To activate microbeads for targeting a specific miRNA, biotinylated cDNA probes are mixed with streptavidin coated Dynabeads (Invitrogen). **(B)** Activated beads are then introduced into solution and bind with complementary strands which enables separation with an external magnetic force **(C).** The beads are then heated in elution buffer to recover the miRNA for spotting on the ARIA sensor **(D)**.

To perform magnetic bead enrichment for miR-181a, total miRNA was extracted from growth media collected from 70% confluent CP70 and A2780 cell lines using the mirPremier microRNA isolation kit (Sigma, St. Louis, Mo). Briefly, conditioned growth media was spun down at 16,000g for 1 minute to ensure removal of all cellular material and then mixed with 1.1 volumes of 100% Ethanol (Sigma, St. Louis, Mo). This mixture was then mixed by inversion,

and centrifuged at 16,000g for 30 seconds in a silica column to bind all small RNA. The column was then washed 3 times in an ethanol based wash solution (16,000g, 30 seconds), dried (16,000g, 30 second) and eluted in DI water (16,000 g, 1 minute) by centrifugation, yielding 50 µL of total miRNA (2-4 ng/µL). To perform magnetic screenings for specific miRNAs from this volume, 4µL volumes of total miRNA sample from each cell line were then added to 50 µL 1X BW buffer solutions of microbeads functionalized with probes for miR-181a (3'–btn-TTTTTTTTTT-ACTCACCGACAGCGTTGAATGTT–5') and miR-134 (3'–btn-TTTTTTTTTT-CCCCTCTGGTCAACCAGTCACA–5'), vortexed for 2-3 minutes, and incubated on a LabQuake rotator at 45-50^{o} C for 50 minutes. A 50-µL solution of cDNA beads mixed with a 4-µL of a 6.25 ng/µL solution of complementary synthetic ssDNA and a second 50-µL solution of cDNA-functionalized beads (no ssDNA) served as positive and negative controls, respectively. To elute the captured ssDNA, the beads (bound with ssDNA targets) were magnetically separated, resuspended in 50µL of 0.25x SSC buffer, and incubated at 68^{o} C for 5 minutes to denature the ssDNA from the cDNA probe. Measuring the concentrations of free ssDNA after elution, we find 2.5 ng/µL in the positive control (~40% recovery) and less than background in the negative control, indicating recovery of the target strand and negligible loss of cDNA from the microbead during elution. We note some of the target strand was in fact lost in this procedure, which was most likely due to experimental conditions designed to minimize nonspecific binding for ARIA measurements.

Since target miRNA concentrations for each cell line were well below the detection limit of the nanodrop system, RT-PCR analysis was performed to validate the magnetic bead enrichment procedure as specific to miR-181a and miR-134. To verify enrichment, we computed the difference in fold change of Ct values (ΔCt) for miR-181a and RNUB6 before and after

enrichment and computed the ratio of ΔCt before and after enrichment; this is the enrichment factor. RT-PCR results generated an enrichment factor of 6.4 (Figure 6A), confirming specificity of the microbead extraction process. By contrast, miR-134 expression levels were undetectable by RT-PCR (Ct > 40, data not shown).

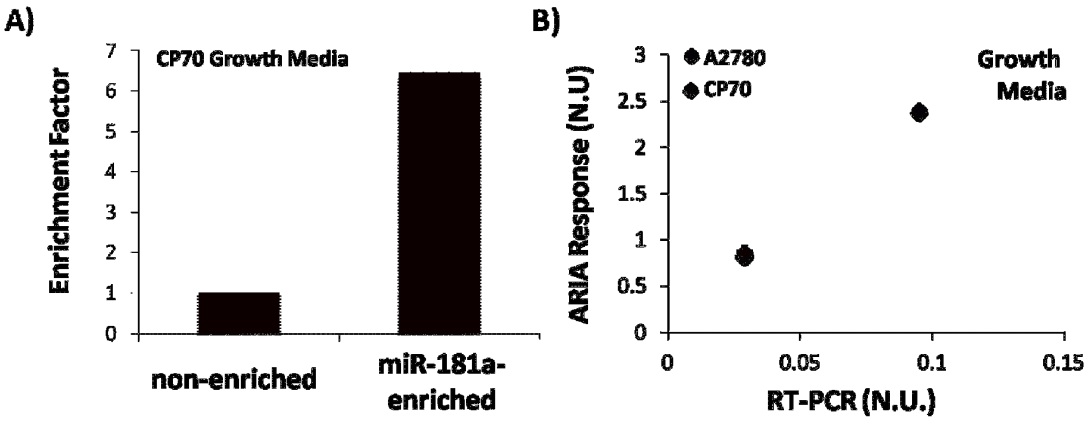

Figure 6. ARIA tests on ovarian cancer cell lines. **(A)** Relative fold change comparing expression of miR-181a against non-targeted RNU6B during the magnetic bead process, verifying enrichment of miR-181a extracted from CP70 growth media. Enrichment factor was determined by computing the ratio of the fold change relative to RNUB6 before and after magnetic bead extraction. **(B)** ARIA shifts for miR-181a normalized to the shift for miR-134 (normalized units, N.U.) and plotted against corresponding RT-PCR values for miR-181a normalized against RNU6B. (miR-134 was undetectable (Ct > 40) by RT-PCR). All points indicate averages of at least 3 samples and standard error bars represent the standard error in the measurement.

Enriched miR-134 and miR-181a samples were then measured in triplicate on the ARIA platform and Δw_p values were extracted as described above. Normalized ARIA responses were

computed by calculating the percentage change in Δw_p for miR-181a relative to miR-134 for CP70 and A2780 growth media extractions. A plot directly comparing the RT-PCR and ARIA measurements, shown in Figure 6B, indicates a direct correlation for miR-181a and RT-PCR data, which is consistent with RT-PCR results and therefore validates the ARIA concept for detection of a miRNA biomarker linked to cisplatinum resistance.

Serum screening for tumor burden biomarker miR-9

Given the ability of the ARIA technology to detect sub-femtomolar amounts of miRNA at or below the detection limit of RT-PCR, we next assessed whether we could detect serum miRNA in a pre-clinical mouse model of ovarian cancer. In this procedure, 50μL serum samples were collected from nu/nu immune-compromised mice which were intraperitoneally implanted with the human SKOV3 ovarian cancer cell line (see supplemental S3 for details). All mice were euthanized after 3 weeks and approximately 1mL of blood was collected through cardiac puncture from the posterior vena cava in order to isolate serum. Additionally, total tumor weight of all intraperitoneal tumors was measured in order to assess total tumor burden in each mouse and correlate that with miRNA's known to be associated with increasing stage in patients (see supplemental section S3 for additional information).

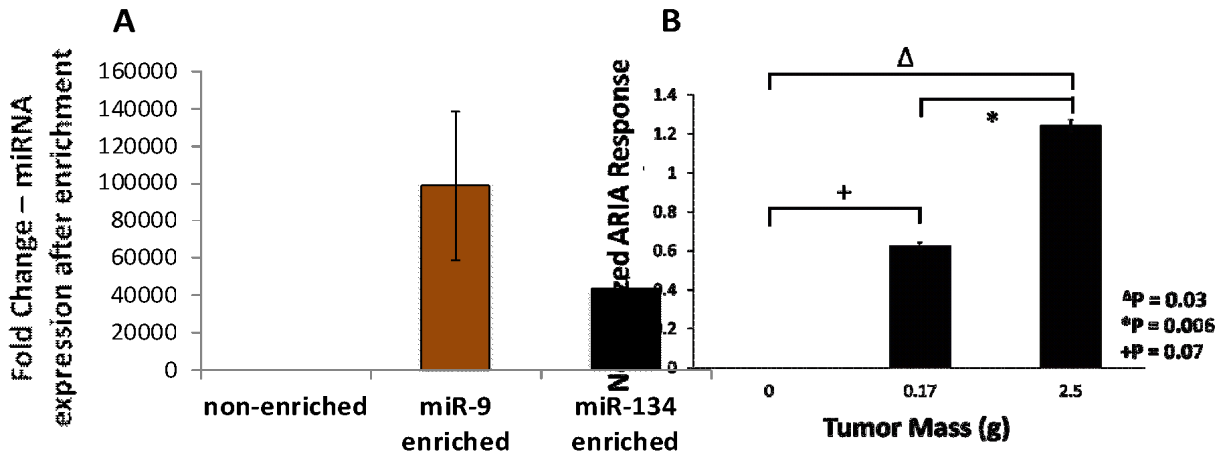

Figure 7. ARIA measurements of miR-9 in mouse serum. (A) A plot comparing concentration of miR-9 before and after magnetic bead extraction, indicating an enrichment factor of 98,000-fold. Fold change was computed by comparing average Ct values (n = 3) to reference RNU6B before and after extraction. **(B)** ARIA measurements on miR-9-enriched samples for no tumor, low tumor (0.17g), and high tumor (2.5 g) burden indicate miR-9 circulating in serum can be used as a biomarker for distinguishing mice with high human epithelial ovarian cancer tumor burden from those with low tumor burden ($p = 0.006$) and normal mice ($p = 0.03$). Measurements represent the normalized shift relative to the mouse with no tumor burden. Each point represents the average of 3 ARIA screenings on a single serum sample and error bars correspond to standard errors in the measurement. For Taqman miRNA analysis, real-time PCR was performed using according to the manufacturer's instructions. TaqMan probes for miR-9 and RNU6B were purchased from Applied Biosystems.

ARIA measurements were performed for miR-9 (microbead probe: 3' – btn-TTTTTTTTT-TCATACAGCTAGATAACCAAAGA–5'), whose expression is known to change with increasing ovarian cancer tumor burden [28] in 3 mice which had a tumor burden of 0,

0.17g, and 2.5g. ARIA measurements were determined by performing measurements in triplicate and computing average Δw_p values computed as described in the previous section. Normalized ARIA measurements were computed by calculating the percentage shift in ARIA measurement for low and high tumor burden samples relative to serum sample measurements extracted from the mouse with no tumor burden.

To confirm successful miRNA enrichment, Taqman RT-PCR was performed on miRNA isolated from serum before and after enrichment of miR-9. Remarkably, when compared to a highly expressed RNU6B, miR-9 was increased 98,000-fold after target enrichment (Figure 7A). Although Taqman RT-PCR was able to detect miR-9 expression, the Ct values were near the detection limit and therefore unable to discriminate between high and low tumor burden determine (data not shown). However, ARIA was able to detect divergent concentrations of miR-9 in the mice according to tumor burden ($p=0.03$) (Figure 7B). Taken together these data indicate ARIA performance is superior in sensitivity to RT-PCR.

In conclusion, the results presented in this work successfully demonstrated ARIA as an efficient method for assessing miRNA biomarkers in plasma serum that exceeds the sensitivity of RT-PCR and enables rapid measurement without the use of enzyme based amplification and expensive fluorophores. This system successfully demonstrated highly sensitive detection of clinically relevant ovarian cancer biomarkers extracted from serum and growth media using magnetic bead extraction technology and results were validated by and consistently exceeded that of RT-PCR. The design of ARIA technology and the simplicity of extraction process will enable integration into systems including microfluidic devices and robotic fluid handling platforms permitting high-throughput analysis of multiple miRNA panels for various diagnostic applications.

This material is available free of charge via the Internet at http://pubs.acs.org.

AUTHOR INFORMATION

Corresponding Author

* Email: rpurnell@chromologic.com. Phone: 626-381-9974

ACKNOWLEDGMENTS

A2780 and CP70 cell lines were a kind gift from Dr. Paul Modrich (Duke University, Raleigh, NC). This work is supported by NIH NCI Contract # HHSN261201100047C

References

[1] Bartel, D. P. *Cell* Jan. 2009, DOI:10.1016/j.cell.2009.01.002

[2] Morales-Prieto, D. M. and Markert, U. R., *J. Reprod. Immunol* Mar. 2011, DOI:10.1016/j.jri.2011.01.004

[3] Guay, C.; Roggli, E.; Nesca, V.; Jacovetti, C.; and Regazzi, R. *Transl Res* Apr. 2011, DOI:10.1016/j.trsl.2011.01.009

[4] Cui, W.; Ma, J.; Wang, Y.; and Biswal, S. *PLoS ONE* Aug. 2011, DOI:10.1371/journal.pone.0022988

[5] Wittmann, J. and Jäck, H.-M. *Biochim. Biophys. Acta* Dec. 2010, DOI:10.1016/j.bbcan.2010.07.002

[6] Mitchell, P. S.; Parkin, R. K.; Kroh, E. M.; Fritz, B. R.; Wyman, S. K.; Pogosova-Agadjanyan, E. L.; Peterson, A.; Noteboom, J.; O'Briant, K. C.; Allen, A.; Lin, D. W.; Urban, N.; Drescher, C. W.; Knudsen, B. S.; Stirewalt, D. L.; Gentleman, R.; Vessella, R. L.; Nelson, P. S.; Martin, D. B.; Tewari, M. *PNAS*, Jul. 2008, DOI:10.1073/pnas.0804549105

[7] Lawrie, C. H.; Gal, S.; Dunlop, H. M.; Pushkaran, B.; Liggins, A. P.; Pulford, K.; Banham, A. H.; Pezzella, F.; Boultwood, J.; Wainscoat, J. S.; Hatton, C. S. R.; Harris, A. L. *Br. J. Haematol.*, May 2008, DOI:10.1111/j.1365-2141.2008.07077.x

[8] Resnick, K. E.; Alder, H.; Hagan, J. P.; Richardson, D. L.; Croce, C. M.; Cohn, D. E.; *Gynecol. Oncol.* Jan. 2009, DOI:10.1016/j.ygyno.2008.08.036

[9] Taylor, D. D.; Gercel-Taylor, C. *Gynecol. Oncol.* Jul. 2008, DOI:10.1016/j.ygyno.2008.04.033

[10] Cortez, M. A.; Calin, G. A. *Expert Opinion on Biological Therapy* Jun. 2009, DOI:10.1517/14712590902932889

[11] Hu, Z.; Chen, X.; Zhao, Y.; Tian, T.; Jin, G.; Shu, Y.; Chen, Y.; Xu, L.; Zen, K.; Zhang, C.; Shen, H. *JCO* Apr. 2010, DOI: 10.1200/JCO.2009.24.9342

[12] Hunter, M. P.; Ismail, N.; Zhang, X.; Aguda, B. D.; Lee, E. J.; Yu, L.; Xiao, T.; Schafer, J.; Lee, M.-L. T.; Schmittgen, T. D.; Nana-Sinkam, S. P.; Jarjoura, D.; Marsh, C. B. *PLoS ONE*. Nov. 2008, DOI:10.1371/journal.pone.0003694

[13] Seefeld, T. H.; Zhou, W.-J.; Corn, R. M. *Langmuir*. May 2011, DOI:10.1021/la200649n

[14] Fang, L. J.; Verkleeren, R.; Scibek, J.; Frutos, A. *Nature Methods | Application Notes*. Mar. 2007, DOI:10.1038/an1794

[15] Fang, S.; Lee, H. J.; Wark, A. W.; Corn, R. M. *J. Am. Chem. Soc.* Nov. 2006, DOI:10.1021/ja065223p

[16] Mares, J. W.; Wei, X.; Weiss, S. M. *Frontiers in Optics Conference*, 2012, DOI: 10.1364/FIO.2012.FW4B.2

[17] Xie, P.; Xiong, Q.; Fang, Y.; Qing, Q.; Lieber, C. M. *Nature Nanotechnology* 2012, DOI:10.1038/nnano.2011.217

[18] Fang, Z.; Kelley, S. O. *Analytical Chemistry*. Jan. 2009, DOI:10.1021/ac801890f

[19] Song, F.; Zhou, F.; Wang, J.; Tao, N.; Lin, J.; Vellanoweth, R. L.; Morquecho, Y.; Wheeler-Laidman, J. *Nucleic Acids Res.* Jul. 2002, DOI: 10.1093/nar/gnf072

[20] Menon, N.; Minelly, J. D. Tag free bio sensing micro strip. U.S. Patent 7,354,772 Apr 8th, 2008.

[21] Menon, N.; Minelly, J. D. Tag free bio sensing micro strip. U.S. Patent 8,142,723, Mar 27th, 2012.

[22] Scrivener, P. L.; Tarbox, E. J.; Maton, P. D. *Electronics Letters*. 1989, DOI:10.1049/el:19890375

[23] Hänel, C.; Gauglitz, G. *Anal Bioanal Chem*. Jan. 2002, DOI:10.1007/s00216-001-1197-3

[24] Fu, D.; Choi, W.; Sung, Y.; Yaqoob, Z.; Dasari, R. R.; Feld, M. *Biomed Opt Express*. Aug. 2010, DOI:10.1364/BOE.1.000347

[25] Gourley, P. L.; Gourley, M. F. *Trends Biotechnol.* Nov. 2000, DOI:10.1016/S0167-7799(00)01496-7

[26] Zhang, H.-H.; Wang, X.-J.; Li, G.-X.; Yang, E.; Yang, N.-M. *World J. Gastroenterol.* May 2007.

[27] Parker, R. J.; Eastman, A.; Bostick-Bruton, F.; Reed, E. *J Clin Invest*. Mar. 1991, DOI: 10.1172/JCI115080

[28] Laios, A.; O'Toole, S.; Flavin, R.; Martin, C.; Kelly, L.; Ring, M.; Finn, S. P.; Barrett, C.; Loda, M.; Gleeson, N.; D'Arcy, T.; McGuinness, E.; Sheils, O.; Sheppard, B.; O' Leary, J. *Mol. Cancer*. 2008, DOI:10.1186/1476-4598-7-35

[29] Fogh, J., *Human tumor cells in vitro*. New York: Plenum Press, 1975.

TOC Graphic:

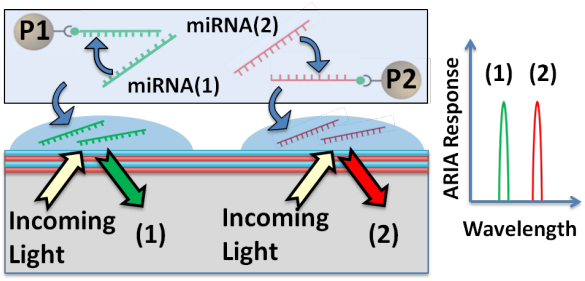
P1
miRNA(2)
miRNA(1)
P2
Incoming Light
(1)
Incoming Light
(2)
ARIA Response
(1) (2)
Wavelength